The Type IIP Supernova 2012aw in M95: accurate photometric and spectroscopic observations of the photospheric phase and hydrodynamical modelling

M. Dall'Ora[1]

M. T. Botticella[1]

M. L. Pumo[2]

L. Zampieri[2]

L. Tommasella[2]

G. Pignata[3]

A. Bayless[4]

T. Pritchard[5]

R. Kotak[6]

C. Inserra[6]

M. Della Valle[1]

E. Cappellaro[2]

S. Benetti[2]

S. Benitez[9]

F. Bufano[XX]

N. Elias-Rosa[XX]

M. Fraser[2]

A. Harutyunyan[7]

E. Y. Hsiao[XX]

T. Ijima[2]

E. Kankare[XX]

P. Kuin[XX]

J. Maund[6]

A. Morales Garoffolo[XX]

N. Morrell[XX]

U. Munari[2]

P. Ochner[2]

A. Pastorello[2]

F. Patat[10]

M. M. Phillips[XX]

P. Roming[XX]

A. Siviero[2]

S. Smartt[6]

J. Sollerman[8]

F. Taddia[8]

S. Taubenberger[9]

S. Valenti

D. Wright[6]

ABSTRACT

We present our extensive optical and near infrared photometric and spectroscopic campaign of the type IIP supernova SN 2012aw. We thickly covered the evolution of SN 2012aw from the explosion up to the end of the photospheric phase, with two additional photometric observations collected during the nebular phase, to estimate the ^{56}Ni mass. We also included in our analysis already

[1]INAF, Osservatorio Astronomico di Capodimonte, Napoli, Italy, dallora@na.astro.it

published Swift UV data. On the basis of our dataset, we estimated all the relevant physical parameters of SN 2012aw with the hydrodynamical code GRRAAL, getting the envelope mass $M_{env} \sim 21 - 23 M_{\odot}$, the radius $R \sim 2.3 - 3.3 \times 10^{13}$ cm ($\sim 330 - 470 R_{\odot}$), the energy $E \sim 1.6 - 1.7$ foe, and an initial ^{56}Ni mass of $0.078 M_{\odot}$. These values are reasonably well supported by the independent evolutionary models mass and radius of the progenitor, and suggest a progenitor mass that may be higher than the observational limit of $16.5 \pm 1.5 M_{\odot}$ of the type IIP events.

Subject headings: supernovae: general —supernovae: individual: 2012aw

1. Introduction

Type II supernova (SN) events are the product of the collapse of a moderately massive progenitor, with initial mass mostly between $\simeq 8_{\odot}$ and $\simeq 30 M_{\odot}$ (e.g. Limongi & Chieffi 2003). Following the classical classification scheme (see Filippenko 1997 for a review) their spectra show prominent Balmer lines, which means that at the time of the explosion they still retained their hydrogen-rich envelope. "Plateau" Type II supernovae (Type IIP SNe) show a nearly constant light curve for $\sim 80 - 120$ days (Barbon et al. 1979). The plateau is thought to be powered by the release of the thermal energy deposited by the shock wave with a minor contribution due the energy released during the recombination of the hydrogen present in the ejeted material (e.g. Kasen & Woosley 2009, Maguire et al. 2010, Pumo & Zampieri 2011). In a few cases the progenitors have been identified in archive high-resolution images and the data suggest that the progenitors are red supergiants (RSGs) of initial mass between $\sim 8 M_{\odot}$ and $\sim 17 M_{\odot}$. Available data show the lack of high-mass progenitors, and this fact has been dubbed the "RSG problem" (Smartt 2009). However, it should be noted that the dust produced in the RSG wind could increase the extinction, with the net effect of underestimating the luminosity and, as a consequence, the mass of the progenitor (Walmswell & Eldridge 2012). In addition, there is evidence that a minor fraction of type II SNe result from the explosion of blue supergiant stars, the best example beeing SN 1987A (Arnett et al. 1989). Indeed, accordingly to Pastorello et al. (2012), $< 5\%$ of all type II SNe are 1987A-like events.

The interest of Type IIP SNe is twofold. First, observations show that IIP SNe are the most common explosions in the nearby Universe. This means that, given their observed mass range, they can be used to trace the cosmic star formation history up to $z \sim 0.6$ (see Botticella et al. 2012; Dahlen et al. 2012). Second, it has been suggested that they can be used as distance indicators up to distances of cosmological interest (see Hamuy & Pinto

2002; Nugent et al. 2006; Poznanski et al. 2009; Olivares E. et al. 2010).

Despite of their frequency and importance, only few Type IIP SNe have been extensively monitored, photometrically and spectroscopically (see, for example, Maguire et al. 2010 for some of the last 20 years observations). Therefore, the occurence of a nearby Type IIP SN offers us an unique opportunity to collect very high quality photometric, spectroscopic and polarimetric data from early stages up to the nebular phase. Through the analysis of pre-explosion images we also have the possibility to compare the progenitor parameters estimated with the hydrodynamical explosion codes, with the predictions of the evolutionary models.

SN 2012aw was discovered by Fagotti et al. (2012) in the spiral galaxy M95 (NGC 3351), at the coordinates $\alpha = 10$h43m53s.76, $\delta = +11$d40'17".9 on 2012 March 16.86 UT. The magnitude at the discovery epoch was $R \sim 15$ mag steeply raising ($R =\sim 13$ mag, by J. Skvarc on March 17.90 UT). The latest pre-discovery image was on March 15.86 UT (Poznanski et al. 2012). These data allow to constrain the explosion epoch that Fraser et al. (2012) assigned to March 16.0 ± 0.8 UT, corresponding to the Julian day 2456002.5. Designation SN 2012aw was assigned after the spectroscopic confirmations (indepently obtained by Itoh et al. 2012 and by Siviero et al. 2012. An early spectrum taken by Munari et al. (2012) on 2012 March 17.77 UT, showed a very hot continuum, without obvious absorption or emission features. Subsequent spectra showed a clear H_α P Cygni profile, indicating a velocity of the ejecta of about 15000 km s^{-1} (Siviero et al. 2012).

SN 2012aw was also observed in X-rays with Swift (Immler & Brown 2012) between March 19.7 and March 22.2 UT, at the luminosity $L_X = 9.2 \pm 2.5 \times 10^{38}$ erg s^{-1}, and on March 24.25 UT (Stockdale et al. 2012) at the radio frequency of 20.8 GHz with a flux density of 0.160 ± 0.025 mJy. A subsequent radio observation on March 30.1 UT at the frequency of 21.2 GHz (Yadav et al. 2012) revealed a flux density of 0.315 ± 0.018 mJy (Yadav et al. 2012), thus confirming a source radio variability. Finally, spectropolarimetric observations with FORS2@VLT suggested a possible quite large intrisic polarization at early phases, possible signature of substantial asymmetries in the early ejecta (Leonard et al. 2012).

A candidate progenitor was promptly identified in archival Hubble Space Telescope data by Elias-Rosa et al. (2012) and by Fraser et al. (2012), as a RSG. A detailed analysis was therefore conducted by Fraser et al. (2012), on a HST image, and multi-band photometry was carried out on both space (HST WFPC2 $F814W$) and ground based (ISAAC@VLT, SOFI@NTT) archive data. By adopting a solar metallicity, their analysis pointed toward a progenitor of initial mass between 14 and 26 $M_\odot$; the estimated effective temperature ranged between 3300 and 4400 K, while the RSG radius was evaluated larger than $500 R_\odot$ and the

luminosity spanning between $L = 10^5 L_\odot$ and $10^{5.6} L_\odot$. We note that the uncertainties in the Fraser et al. (2012) parameters are due mainly to the line of sight extinction estimate, which they evaluate larger than $E(B-V) = 0.4$ mag at the 2σ level and larger than $E(B-V) = 0.8$ mag at the 1σ level. Van Dyk et al. (2012) produced a similar study, where they carefully discussed the infrared photometric calibration and the subtle effects due to the host galaxy *pre-explosion* reddening (which they estimate as $E(B-V) = 0.71$ mag) and to the variability of the RSG. Assuming a solar metallicity, they found a SED consistent with an effective temperature of 3600 K, luminosity of $L \sim 10^{5.21} L_\odot$, radius $R = 1040 R_\odot$ and initial mass between 15 and $20 M_\odot$. After interpolating their adopted tracks (taken from Ekström et al. 2012), they finally suggested a progenitor of initial mass of $\sim 17 - 18 M_\odot$, which is similar to the upper limit of the initial masses for the Type IIP SNe progenitors of 16.5 ± 1.5, as suggested by Smartt et al. (2009). Subsequently, Kochanek et al. (2012) suggested that the Fraser et al. (2012) and the Van Dyk et al. (2012) luminosity (and mass) values of the progenitor may be overestimated, since they adopted for the reddening the classical absorption-to-reddening ratio $R_V = 3.1$, based on an average dust composition. Indeed, Kochanek et al. (2012) pointed out that a massive RSG produces mostly silicates, for which a ratio of $R_V = 2$ seems more appropriate; moreover, some of the stellar light scattered by dust would be re-emitted at optical wavelenghts. In turn, they suggest a progenitor luminosity between $L = 10^{4.8} L_\odot$ and $L = 10^{5.0} L_\odot$ and a mass of $M < 15 M_\odot$.

Finally, we note that an accurate $BVRI$ light curve of SN 2012aw was recently published by Munari et al. (2013), and that photometric and spectroscopic observations were made available by Bose et al. (2013), covering a period from 4 to 270 days after explosion. Munari et al. (2013) carefully discussed the problems related to the homogeneization of photometric measurements obtained at different telescopes, producing an optimal light curve by means of their "lightcurve merging method". Bose et al. 2013 measured the photospheric velocity, the temperature and the ^{56}Ni mass of SN 2012aw; moreover they estimated the explosion energy and the mass of the progenitor star by comparing their data with existing simulations.

The paper is organised as follows: in section 2 we discuss the relevant parameters of the host galaxy M95; in section 3 we present our photometric dataset, analyzing the photometric time evolution and discussing the bolometric light curve, from which we give an estimate of the nickel mass. In section 4 we present the spectroscopic observations, discussing the time evolution of the spectral features, and we derive in section 5 the expansion velocity, the spectral energy distribution and the blackbody temperature evolution. In section 6 we present the results of our accurate hydrodynamical modelling, computed to match the observational parameters of SN 2012aw. Conclusions are presented in section 7.

2. The host galaxy M95

M95 (NGC 3351) is a face-on SBb(r)II spiral galaxy (Sandage & Tammann 1987), with coordinates $\alpha_{2000} = 10h43m57.7s$, $\delta_{2000} = 11h42'12.7''$, belonging to the Leo I Group. The total V-band magnitude is $M_V = -20.61 \pm 0.09$ mag and the total baryonic mass has been evaluated as $M_{tot} = (3.57 \pm 0.30) \times 10^{10} M_{\odot}$ (Gurovich et al. 2010). The distance to M95 has been evaluated with the Cepheids and the tip of the red giant branch (TRGB). A quite wide range of distances have been reported during the years, but the latest estimates are comfortably converging: the HST Key Project gave a Cepheids-based distance of $(m-M)_0 = 30.00 \pm 0.09$ mag (Freedman et al. 2001), in excellent agreement with the TRGB-based distance of $(m - M)_0 = 29.92 \pm 0.05$ mag (Rizzi et al. 2007). This agreement is particularly striking, since it is based on two truly independent distance indicators, because Cepheids are young Population I stars, while the TRGB is a feature of the old Population II. A similar result was also obtained on the basis of the planetary nebulae luminosity function ($(m - M)_0 = 30.0 \pm 0.16$ mag, Ciardullo et al. 2002). In the following, we will use as a distance modulus $(m - M)_0 = 29.96 \pm 0.04$ mag, which is the average of the Cepheids and the TRGB based distances. M95 is known to host a central massive black hole (e.g. Beifiori et al. 2009) and its bulge shows intense star forming activity (e.g. Hägele et al. 2007). The SN 2012aw is located in a southern outer arm, 60″ west and 115″ south of the center of M95. The metallicity at the SN position can be approximately estimated as solar-like (Fraser et al. 2012). To our knowledge, no SN events were recorded in M95 before SN 2012aw. Lastly, we note that its measured redshfit from the HI 21 cm line is $z = 0.002598 \pm 0.000002$ (Springob et al. 2005): we have adopted this value to correct our spectra.

3. Photometry

3.1. Data

An intensive campaign of optical and NIR observations of SN 2012aw with a wide range of telescopes was promptly started immediately after its discovery (2012, March 17), until the end of the plateau and the beginning of the radioactive tail (2012, July 21), when the SN went into conjunction with the Sun. Two additional epochs were collected on 2012, December 26, and on 2013, February 11, during the nebular phase.

Optical $UBVRI$ Johnson-Cousins images were collected with 67/92 cm Asiago Schmidt Telescope (Italy), equipped with a SBIG STL-11000M CCD camera (13 epochs); with the Panchromatic Robotic Optical Monitoring and Polarimetry Telescopes (PROMPT, Chile) array of 0.41 m telescopes, equipped with the Apogee U47p cameras, which employ the E2V

CCDs (33 epochs); with the 2.2m telescope at the Calar Alto Obssrvatory (Spain), equipped with the CAFOS Focal Reducer and Faint Object Spectrograph instrument (2 epochs); with the 1.82m Copernico telescope at Cima Ekar (Italy), equipped with the AFOSC Asiago Faint Object Spectrograph and Camera (2 epochs); with the ESO 3.6m telescope (Chile), equipped with the EFOSC2 ESO Faint Object Spectrograph and Camera (2 epochs); with the 4.2m William Herschel Telescope (WHT, Canary Islands, Spain), equipped with the ACAM Auxiliary Port Camera (2 epochs); with the 2.5m Nordic Optical Telescope (Canary Islands, Spain), equipped with the ALFOSC Andalucia Faint Object Spectrograph and Camera (3 epochs). Two early epochs, collected during the rise branch of the light curve and discussed in Munari et al. (2013), have been included for a better sampling of the early phases.

Optical *ugriz* Sloan data were collected with the PROMPT Telescope (21 epochs); with the 2.0m Liverpool Telescope (Canary Islands, Spain), equipped with the RATCam optical CCD camera (11 epochs); with the 2.0m Faulkes Telescope North (Hawaii, USA), equipped with the FI CCD486 CCD detector (4 epochs).

NIR JHK data were gained with the 0.6m Rapid Eye Mount (REM) Telescope (Chile), equipped with the REMIR infrared camera (11 epochs); with the 1.52m Carlos Sanchez Telescope (TCS, Canary Islands, Spain), equipped with the CAIN infrared camera (8 epochs); with the 3.58m Telescopio Nazionale Galileo (G, Canary Islands, Spain), equipped with the NICS Near Infrared Camera Spectrometer (1 epoch).

Data were pre-reduced by the instruments pipelines, when available, or with standard `IRAF` [1] procedures. Only in few cases, to improve the sky background removal, some NIR images were pre-reduced by means of a `IRAF`-based custom pipeline, which adopts for the background subtraction a two-step technique based on the `XDIMSUM IRAF` package (Coppola et al. 2011).

Photometric measurements were carried out by means of the QUBA pipeline (Valenti et al. 2011), which performs differential PSF photometry on the SN and on selected field stars, after these have been calibrated and used as sequence stars. To this aim, the $UBVRI$ calibrated magnitudes of the sequence stars were defined by averaging the photometric sequence published in Henden et al. (2012) and our measurements obtained with the 67/92cm Asiago Schmidt Telescope; *ugriz* sequence stars were defined on images taken at the LT telescope, during selected photometric nights. We decided to not transform the *ugriz* dataset in the $UBVRI$ system, because the current state-of-the-art transformations (Jordi et al. 2006),

[1]IRAF is distributed by the National Optical Astronomical Observatory, which is operated by the Association of Universities for Research in Astronomy, Inc., under cooperative agreement with the National Science Foundation

which are computed for normal field stars, may be not accurate for SNe, strongly dominated by intense absorptions and emissions, which significantly alter the blackbody energy distribution [2]

NIR data were calibrated by adopting four well measured Two Microns All Sky Survey (2MASS) sequence stars. We did not correct for the color terms, since they are generally very small in the NIR bands (e.g. Carpenter 2001) and the uncertainties of the photometric measurements were significantly larger than the uncertainties related to neglecting the color term. Because of the small field of view, data coming from the TCS telescope were measured by means of aperture photometry, since only one sequence star was available, producing a not accurate evaluation of the PSF model. However, we explicitly note that the SN is located far from host galaxy high density regions, and we do not expect a meaningful contamination of the background by the host galaxy contribution. Therefore, plain aperture photometry is expected to be accurate.

Table 7 lists the positions and the photometric properties of the adopted sequence stars, while a map of SN 2012aw and of the reference star is shown in figure 1. The photometry of the SN 2012aw is reported in tables 2, 3 and 4 in the $UBVRI$, $ugriz$, and JHK systems, respectively. Reported photometric uncertainties are computed taking into account the photometric errors and the uncertainties in the calibrations. When multiple exposures were available in the same night for the same filter, the adopted error was the rms of the measured magnitudes with respect to their average.

3.2. Time Evolution

Figures 2, 3, and 4 show the photometric evolution of the SN 2012aw in the Johnson-Cousins, SDSS and NIR photometric systems, respectively. Errorbars were typically smaller than the symbol size, except for the NIR plot. Solid curves represent the fits to the observed data points, evaluated generally by means Chebyshev polynomials with the `CURFIT IRAF` task. The order of the fit was allowed to vary, to minimize the rms. Fit rms was generally of the order of ~ 0.03. In few cases (U, u, and NIR bands) the sampling was poor and we adopted a cubic spline. The last two points, collected in the SN nebular phase, were not included in the fit. The plotted light curves show that the SN was discovered well before the V-band maximum, estimated at the Julian day 2456011.8 ± 0.5. A comparison

[2]The transformations between these two photometric systems may lead to systematic errors in the $u - g$ colour even for normal field stars, as the $u - g$ colour is particularly sensible to temperature, surface gravity, and metallicity (e.g. Lenz et al. 1998).

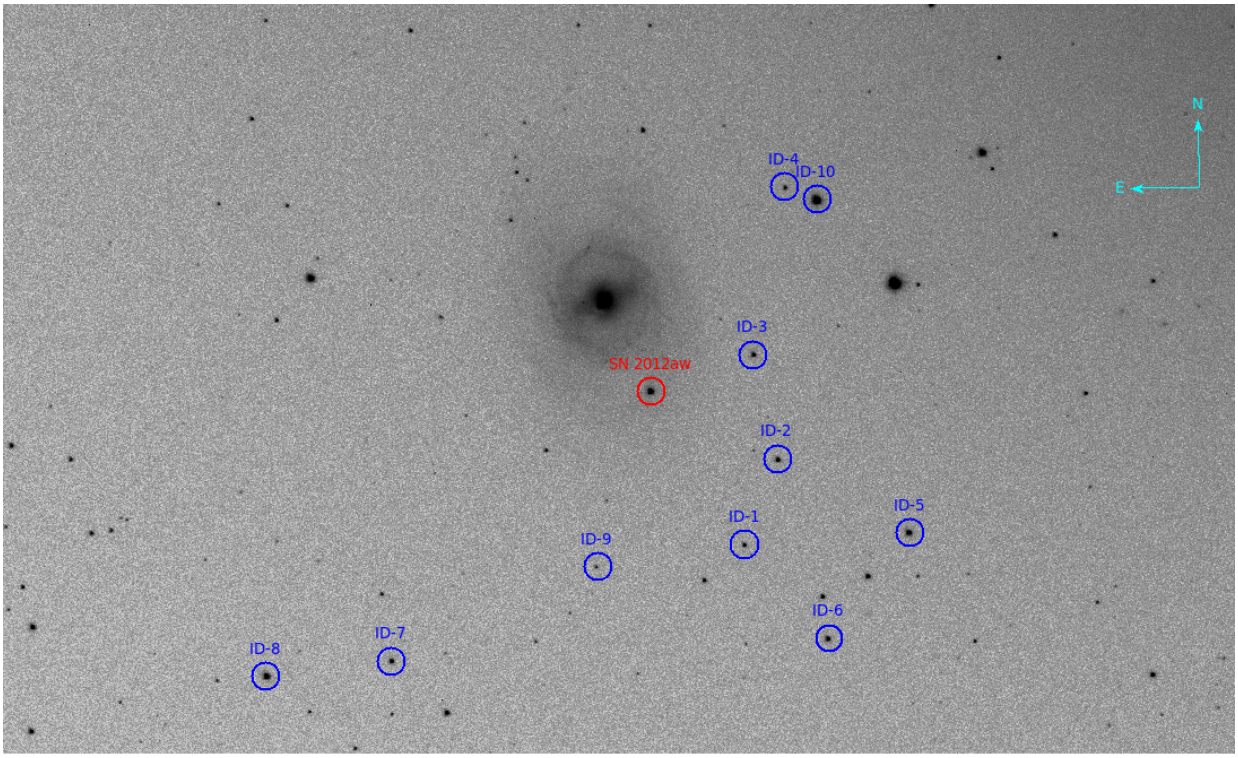

Fig. 1.— Finding chart of SN 2012aw and of the reference stars. V-band image collected at the 67/92cm Asiago Schmidt Telescope on 2012, March 20.

of the early spectra of SN 2012aw with the collection of spectra available in the web tool GELATO (Harutyunyan et al. 2008) indipendently confirms our estimate about the epoch of the explosion. In the following, we will adopt the epoch of the explosion as reference (Day 0). While in the Johnson U and B the light curves show a steady decline from the explosion and from the B maximum (at Day ~ 7), V, R and I bands do show a typical plateau behavior of the Type IIP events. The plateau lasts for ~ 100 days, followed by a bending which marks the fall from the plateau stage. The Sloan photometry is consistent with such a behavior. Finally, the NIR J,H,K photometry shows a steady brightening up to the Day 64, with a behavior similar to other Type IIP supernovae (e.g. SN 2005cs, Pastorello et al. 2009). The apparent drop at the Day ~ 95 could be an artefact, due the poor quality of the data, since it is based on TCS images, where only one reference star was available.

Figure 7 shows the $U-B$, $B-V$, $V-R$ and $V-I$ colour evolution of SN 2012aw during the photospheric phase, compared to other literature SNe. Colours have been deredenned (see sec.3.3), for a proper comparison. The colour evolution appears to be very similar to the other bright SN 1999em (Elmhamdi et al. 2003), SN 2009bw (Inserra et al. 2012) and SN 2005ay (Bufano et al. 2007). The plots are referred to the maximum of the bluest band, since this parameter was best constrained for all the SNe. The plots show that SN 2012aw follows the very typical evolution of the common Type IIP events, with a rapidly increasing of the $B-V$ colour in the first 40 days, followed by a flattening of the curve. There is some hint of a redder color of SN 2012aw at the end of the photospheric phase, that is after ~ 100 days. The same is seen in the $V-I$ colour evolution, while the colours $U-B$ and $V-R$ do nicely follow the bright other Type IIP behavior.

Figures 9 shows the Sloan $g-r$ colour evolution. We compared SN 2012aw with SN 2009kf, for which Sloan photometry is available (Botticella et al. 2010).

Finally, figure 8 depict the time evolution of the near infrared colours and $J-H$, $J-K$. For comparison purposes, we also show the color curves of SN 1999em (Elmhamdi et al. 2003) and of SN 2007od (Inserra et al. 2011), for which the time coverage in the NIR bands was satisfactory. The plots show a quite large scatter, neverthless the values and behavior are similar to those of the two reference SNe.

3.3. Reddening

Photometry was corrected for reddening, both Galactic and in the host galaxy. The Galactic reddening was estimated by using the Schlegel et al. (1998) maps, obtaining a value of $E(B-V) = 0.028$ mag. The internal reddening was estimated on the basis of the

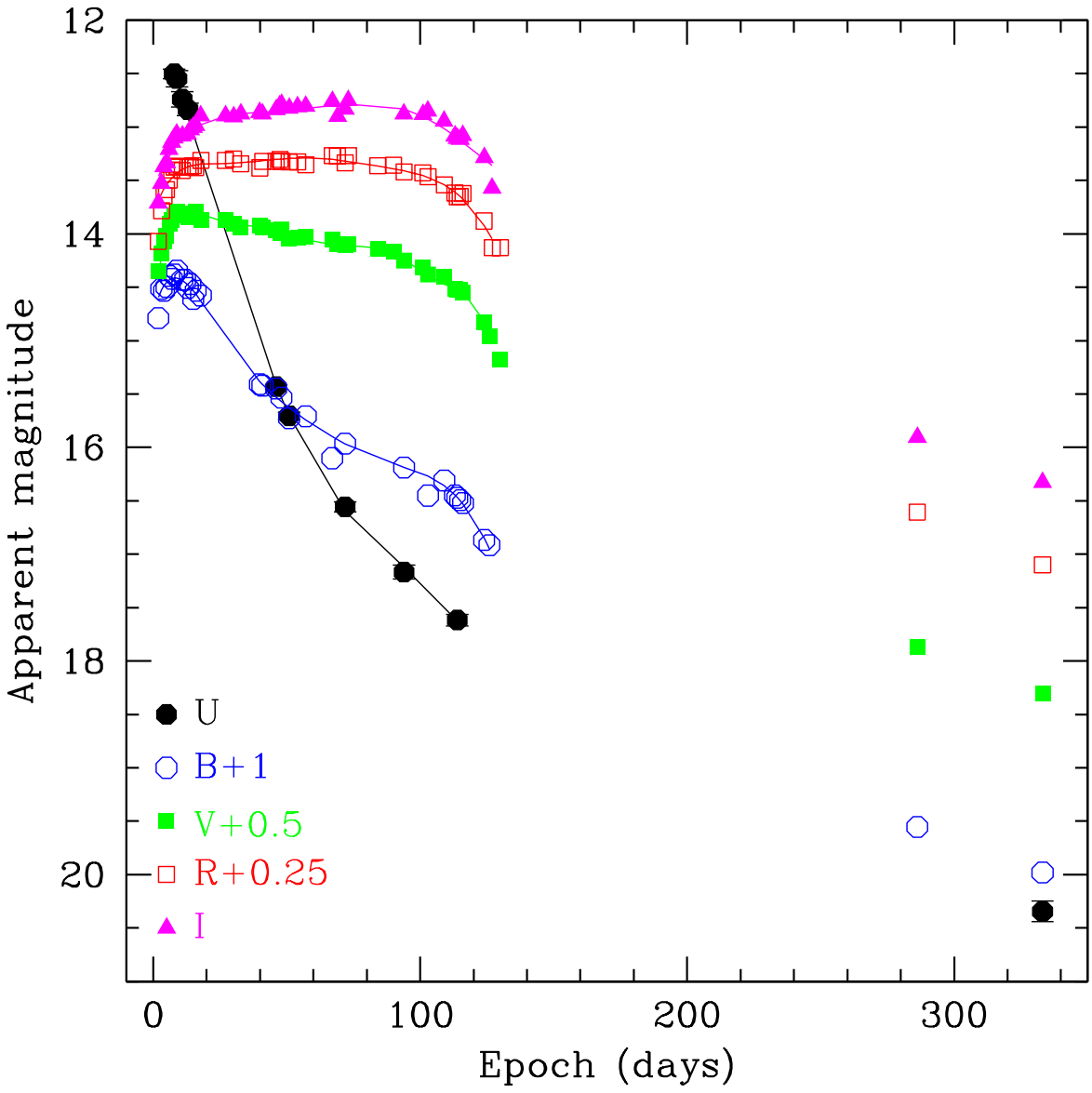

Fig. 2.— Photometric evolution in the $UBVRI$ system. Individual light curves were shifted for clarity.

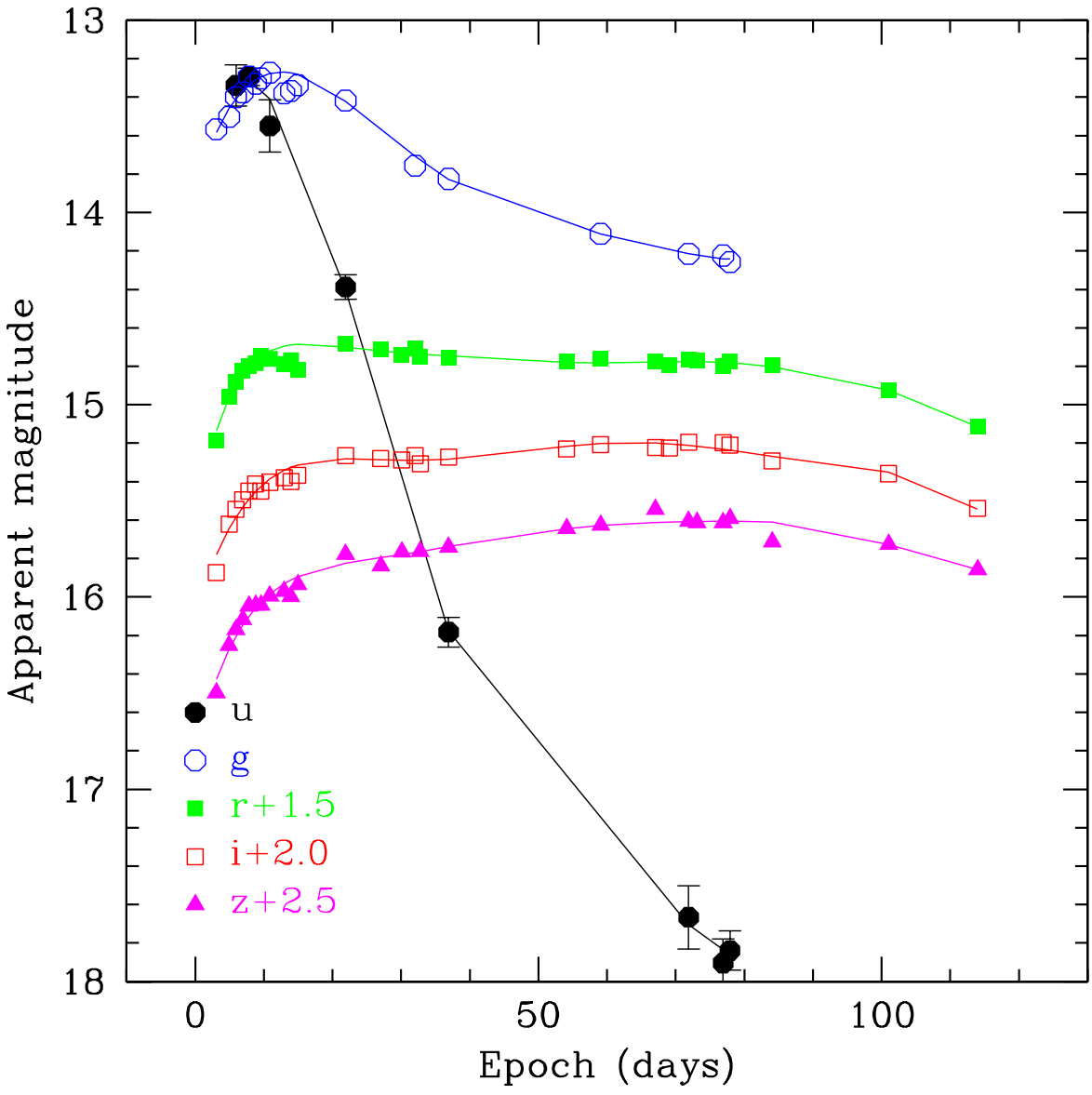

Fig. 3.— Photometric evolution in the *ugriz* system. Individual light curves were shifted for clarity.

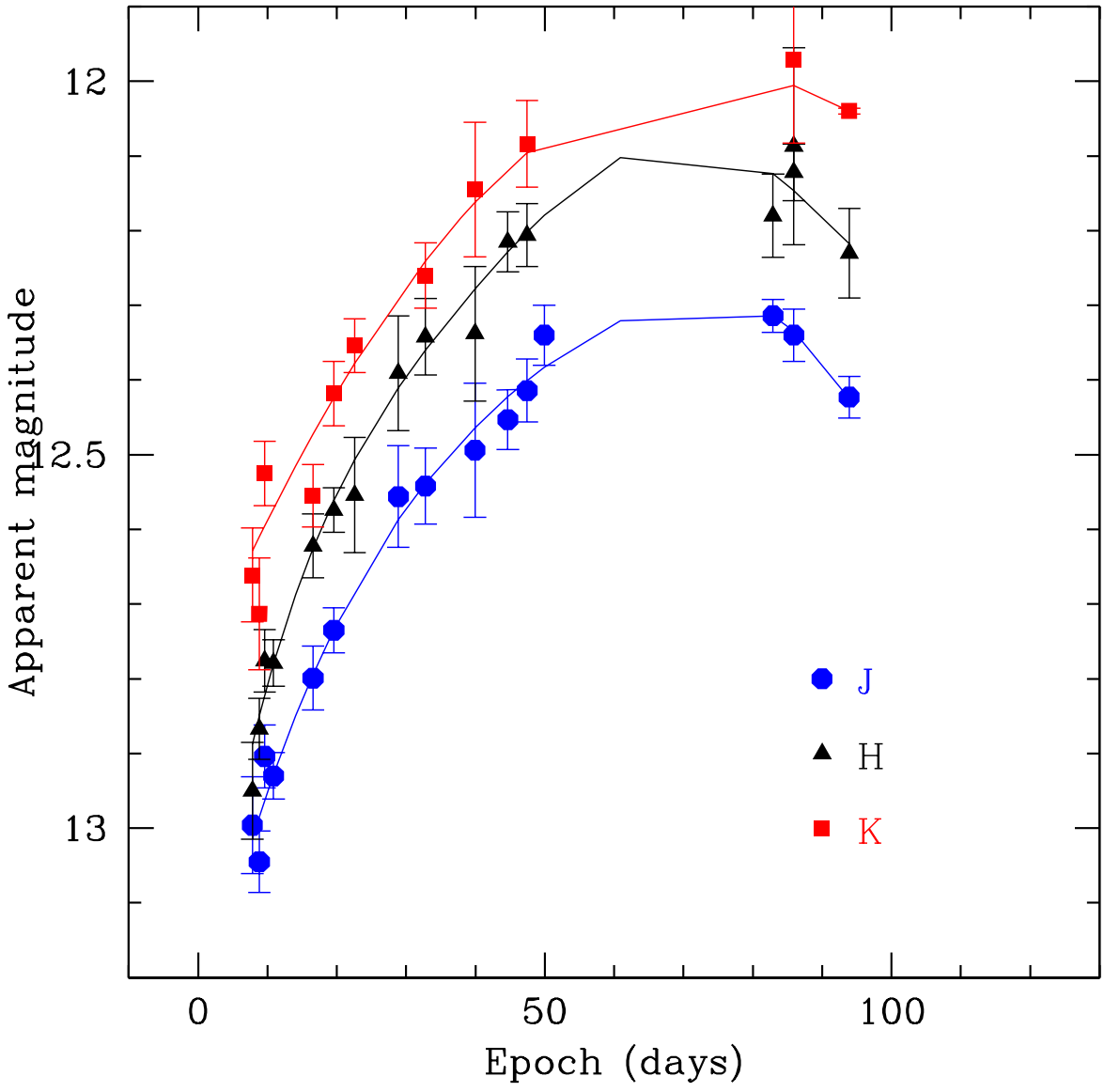

Fig. 4.— Photometric evolution in the JHK system.

NaID equivalent width (EW) on a SARG@TNG high-resolution spectrum. We measured EW(D2 λ5909.33) = 286 ± 17 mÅ and EW(D1 λ5915.32) = 240 ± 16 mÅ, obtaining a column density of $log(NaI) = 12.80 \pm 0.14$. Following Ferlet et al. (1985) this translates into $log(H) = 21.05 \pm 0.14$ and, according to Bohlin et al. (1978), in the colour excess $E(B-V) = 0.19 \pm 0.06$, which transforms in the relatively high host absorption of $A(B)_h = 0.79 \pm 0.25$ mag, by assuming a Galactic $R_V = 3.1$ total-to-selective absorption ratio (Cardelli et al. 1989). We explicitly note that this value is in agreement with the $E(B-V) = 0.15$ mag upper limit given by Bose et al. (2013), on the basis of the blackbody fit to the early observed fluxes. Moreover, it is interesting to note that our measurements are, within the uncertainties, in excellent agreement with those obtained by Van Dyk et al. (2012), of EW(D2 λ5909.33) = 269 ± 14 Å and EW(D1 λ5915.32) = 231 ± 11 Å. Van Dyk et al. (2012) derived a significantly lower reddening, of $E(B-V) = 0.055 \pm 0.014$ mag, by adopting the Poznanski et al. (2012) calibration. This gives a host absorption of $A(B)_h = 0.23 \pm 0.04$ mag (Cardelli et al. 1989), sensibly lower than our estimate at the 1σ level, but in marginal agreement at the 2σ level.

For an independent check, we decided to resort on the "color-method" (Olivares E. et al. 2010). This method relies on the assumption that, at the end of the plateau, the intrinsic $V-I$ color is constant, and a possible color-excess is only due to the host galaxy reddening (having corrected for the Galactic reddening). According to their eq. (7)

$$A_V(V-I) = 2.518[(V-I) - 0.656] \quad (1)$$

$$\sigma(A_V) = 2.518\sqrt{\sigma_{(V-I)} + 0.053^2 + 0.059^2} \quad (2)$$

and following the prescriptions described in their paper, we adopted in the above formulas the $(V-I)$ colour at Day ~ 100, which is roughly ~ 15 days before the end of the plateau. We derive $A(V)_h = (0.83 \pm 0.10)$ mag, which corresponds to $A(B)_h = 1.11 \pm 0.13$ mag (Cardelli et al. 1989), thus supporting a high internal reddening correction. For the following discussion, we will therefore adopt our high-resolution spectrum-based estimate, i.e. of $A(B)_h = 0.79$ mag.

3.4. Bolometric light curve and ^{56}Ni mass

The bolometric light curve (Fig. 10) was obtained by integrating our photometric measurements and the SWIFT UV photometry (Bayless et al. 2013), and using the above adopted reddening and the distance modulus. In detail, a bolometric light curve was obtained by first

converting $uvw2uvw1UBVRIJHK$ magnitudes into monochromatic fluxes per unit wavelength, then correcting these fluxes for the adopted extinction according to the extinction law from Cardelli et al. (1989), and finally integrating the resulting spectral energy distribution (SED) over the range of wavelength, after assuming zero flux at the integration limits. We estimated the flux only for the phases in which V band observations were available. The photometric data in the other bands were estimated at these phases by interpolating magnitudes in adjacent nights. The estimated luminosities are shown in table XXX. The peak of the bolometric luminosity is reached about at Day ~ 8 at a luminosity of $L_{bol} = 7.294 \times 10^{42}$ erg s^{-1}. In order to compare SN 2012aw with other literature SNe, for which a limited wavelength coverage was available, we calculated a $UBVRI$ pseudo-bolometric light curve of SN 2012aw. The comparison, in Fig. 11 of SN 2012aw with SN 1992H, (Clocchiatti et al. 1996); SN 1999em, (Elmhamdi et al. 2003); SN 2009bw, (Inserra et al. 2012); SN 2004et (Maguire et al. 2010), shows that SN 2012aw is one of the brightest Type IIP events. ^{56}Ni mass was estimated by comparing, during the nebular phase, the luminosity of SN 2012aw with that of SN 1987A, assuming a similar $\gamma-$rays deposition fraction and by scaling comparing the SN 2012aw and SN 1987A luminosities, one derives:

$$M(^{56}Ni)_{12aw} = M(^{56}Ni)_{87A} \times \frac{L_{12aw}}{L_{87A}} M\_odot \tag{3}$$

where the luminosities must be compared at similar epochs. We adopted for SN 1987A a ^{56}Ni mass of $M(^{56}Ni)_{87A} = 0.073 \pm 0.012 M_{\odot}$, which is the weighted mean of the values given by Arnett & Fu (1989) and by Bouchet et al. (1991), and the ultroviolet-optical-infrared bolometric luminosity given by (Bouchet et al. 1991). We therefore obtained $M(^{56}Ni)_{12aw} = 0.068 \pm 0.013 M_{\odot}$, as average of the individual estimates at Days 286 and 333. This value is in agreement, within the uncertainties, to the estimate of $0.06 \pm 0.01 M_{\odot}$ given by Bose et al. (2013).

The estimated nickel mass can be compared with the values of our comparisons SNe, that range from $\sim 0.02 M_{\odot}$ (1999em, Elmhamdi et al. 2003; 2009bw, Inserra et al. 2012) to $\sim 0.06 M_{\odot}$ (2004et, Maguire et al. 2010 and $\sim 0.07 M_{\odot}$ (1992H, Clocchiatti et al. 1996). All the estimates were produced in the original papers by adopting the same method we adopted for SN 2012aw, except for 1992H, whose ^{56}Ni mass was estimated from the theoretical light curve.

4. Spectroscopy

4.1. Spectroscopic observations and data reduction

Spectroscopic data were collected approximately in the first three months of SN 2012aw evolution. Table 5 lists the journal of the spectroscopic observations, with the instruments and the instrumental setups. Spectra were pre-reduced in a standard fashion (overscan and bias subtraction, trimming, flat-fielding) by using the tools available in `IRAF`. Wavelenght calibration was carried out with the same instrumental setup used for the science obsservations. Calibrated spectra were corrected for the heliocentric recession velocity of the host galaxy. Flux calibration was performed by comparison with selected spectrophotometric standard stars, during the same nights of the scientific observations and with the same instrumental setup. Finally, absolute flux calibration was verified by comparing to integrated flux measured in the $UBVRI$ bands, with the corresponding photometric measurements (with the `IRAF` package `CALCPHOT`). When the spectra were collected in nights for which no photometry was available, a simple average of the photometric measurements was adopted or, if the spectrum was not bracketed by two consecutive photometric measurements, by adopting the magnitude estimated by the photometric fit, discussed in the previous section. After the correction, the difference between the spectral magnitudes and the photometric magnitude were in the range between 0.01 and 0.05 mag. The same procedure was adopted for the NICS near-infrared spectra, but in this case by considering the Cousins I and the JHK NIR bands. It is worth noticing that `CALCPHOT` adopts the Bessell & Brett (1988) NIR photometric system, while our photometry was calibrated into the 2MASS system. We therefore transformed the `CALCPHOT` synthetic photometry into the 2MASS system following Carpenter (2001). Finally, we corrected the photometry-corrected spectra for the adopted reddening.

4.2. Spectral Time Evolution

Figure 12 shows the optical spectral evolution of SN 2012aw, with the phases referred to epoch of the explosion. The first spectrum, few hours after the estimated explosion, exhibited an almost featurless hot continuum. Interestingly enough, a "bump-shaped" feature is clearly visible at about 4600 Å. This feature fades very quickly, and it is no longer visible at the epoch of V maximum (Day $\sim$ 9). A similar feature was also reported and discussed for SN 2009bw (Inserra et al. 2012). A possible interpretation for such a feature, points toward a blend of highly ionized C and N features (also discussed for the IIn event SN 1998S Fassia et al. 2001). The second spectrum, collected on Day $\sim$ 3, shows the emergence of the typical

broad H_α feature, as well as the HeI feature at ~ 5876 Å. At the epoch of V maximum (Day ~ 9), the H_α, H_β, H_γ and H_δ lines are clearly visible. Typical SN IIP metal lines are visible in the blue part of the spectra after the V maximum, namely the Fe II, Ti II, Sc II, Ba II, and Ca II HK features. As the ejecta expand (from Day 24), the continuum becomes fainter and redder in the UV-blue part of the spectra, while other features appear at wavelengths longer than 5000 Å. In particular, the sodium doublet NaID ($\lambda\lambda 5890, 5896$ Å) does appear, possibly blended with Ba II. In the red part, a strong Ca II P-Cygni feature outstands at ~ 8570 Å at Day 24, which from Day 29 deblends into three features at 8498 Å, at 8542 Å, and at 8662 Å. A full atlas of the identified features is shown in figure 13, at relevant phases.

Figure 14 shows the NIR infrared evolution, again with the phases referred to the epoch of explosion. The first spectrum has been masked in correspondance to the regions of low atmospheric transmission that resulted very noisy. Our time coverage goes from Day 15 to Day 53. The Paschen series is clearly visible at all reported phases, with the Pa_γ possibly blended with the He I. A possible blend of the Brackett Br_γ line with the Na I is also visible in all the spectra. Interestingly, Paschen Pa_γ and Pa_δ features seem to show a small hump in absorption that, if confirmed, could suggest the presence of circumstellar material. Redward of the Ca II line, is visible the Fe II line, which could be blended with the Paschen Pa_ϵ line. Finally, we note the development of an unidentified emission on Day 24 at $\sim 10400 \mathring{A}$. Searching for a possible identification we consulted the National Institute of Standards and Technology archive [3] and the `SYNOW` spectral synthesis code (e.g. Millard et al. 1999, Branch et al. 2002; Parrent et al. 2007 for the `SYNOW` 2.0 description), but we could not find a reasonable match with usual SN ions. Therefore we suggest that this is a high velocity feature of the Pa_γ line. This feature clearly splits in two components in the Day 46 spectrum, at 10340 Å and 10560 Å that, with the above identification, would correspond to velocities of ~ 16000 and ~ 10000 km s^{-1}, respectively.

5. Expansion velocity, black body temperature and SED evolution

Figure 15 shows the evolution of the photospheric expansion velocities measured from the Doppler-shift absorption minima of the Hα, Hβ Fe II(λ5169 Å), Sc II(λ6246 Å) and Ca II (λ8520 Å) lines, starting from the epoch of the explosion. Measurements have been performed by means of the `IRAF` task `SPLOT`. The Hα and Hβ lines are characterized by the highest velocities, starting from ~ 14000 and ~ 12000 km s^{-1}, respectively. Their velocities rapidly decrease and, at about 50 days from the explosion, they reach an almost constant

[3] http://www.nist.gov/pml/data/asd.cfm

value of $\sim$ 7000 and $\sim$ 5000 km s^{-1}, respectively. We note that these values appear fairly large, since for other SNe the velocities at same epochs appear lower (e.g. SN 2009bw, Inserra et al. 2012; SN 2004et Maguire et al. 2010). As is typical in Type IIP SNe, Hα and Hβ velocities are higher, since these spectral features form at larger radii than most metal lines. The Fe II and the Sc II velocities are taken as better tracers of the photospheric velocities, since the relevant transitions have small optical depths. They show a very similar behavior, supporting the identification of these spectral features, and they both settle to $\sim$ 3000 km s^{-1} after about two months. A very similar behaviour is shown also by othe luminous Type IIP SNe, such as SN 2009bw (Inserra et al. 2012), while the velocities of the same features of other well-studied Type IIP SN such as SN 2004et, SN 1999em and SN 2005cs appear substantially lower (e.g. Maguire et al. 2010, their figure 21). Finally, the Ca II feature shows a very similar behaviour to that of Fe II and Sc II, but with a slightly larger scatter, due to the measurement uncertainties.

Figure 16 shows the time evolution of the photospheric temperature, evaluated with a blackbody fit to the photometric data (blue filled triangles) and to the spectral continuum (red open boxes). In the first $\sim$ 20 days, photometry-based temperatures do appear sistematically hotter than the spectral-based measurements, while later on Day 25, the measurements agree within the uncertainties. The behaviour of the spectral continuum temperatures looks similar to other Type IIP SNe (e.g. Inserra et al. 2012, Fig. 11). Interestingly, Fig. 16 shows a constant temperature from Day $\sim$ 30, in agreement with the Bayless et al. (2013) findings.

Figure shows the SED evolution, between Day $\sim$ 4 and Day $\sim$ 132. Our SED was based on the optical-NIR photometry, already discussed, complemented with Swift UV $uvw2$ and $uvw1$ data (Bayless et al. 2013), which cover approximately the first 100 days after explosion. Our spectral coverage is therefore between $\sim$ 2000 Å and $\sim$ 22000 Å. During this time, the optical-NIR fluxes in the range $\sim$ 4000$-$ $\sim$ 22000 Å can be be reproduced by a single blackbody curve. However, shortwards of $\sim$ 4000 Å, the SED does not seem to follow the blackbody profile, but shows a higher flux. This behavior could be due to the presence of strong emission line in the UV part of the spectrum. In fact, the UV spectra collected with Swift(Bayless et al. 2013), which span from Day 5 to Day 30, do show quite prominent emission features bluer than $\sim$ 3000 Å, but in the range $\sim 3200 - 4000$ Å Swift spectra do not show any strong emission line. Therefore, we suspect that this observed "blue up-turn" is due to the well-known read leak of the Swift $uvw2$ and $uvw1$ filters, with a significant trasmissivity redward of 3000 Å.

6. Explosion and progenitor parameters

We estimate the physical properties of the progenitor of SN 2012aw at the explosion (namely, the ejected mass, the progenitor radius and the explosion energy) by performing a simultaneous χ^2 fit of the main observational quantities (i.e. bolometric light curve, evolution of line velocities and continuum temperature at the photosphere) against model calculations, using the same well-tested procedure adopted for modelling other observed CC-SNe (e.g. SNe 2007od, 2009bw, and 2009E; see Inserra et al. 2011, Inserra et al. 2012, and Pastorello et al. 2012).

Two codes have been used to calculate the models: the semi-analytic code described in Zampieri et al. (2003) and the General-Relativistic, RAdiAtion-hydrodynamics Lagrangian (`GRRAAL`) code described in Pumo et al. (2010) and Pumo & Zampieri (2011). The first one solves the energy balance equation for a spherically symmetric, homologously expanding envelope of constant density. It is used to perform preparatory studies aimed at individuating the parameter space describing the CC-SN progenitor at the explosion and, consequently, to guide the more realistic, but time consuming simulations performed with the `GRRAAL` code. `GRRAAL` is able to simulate the evolution of the physical properties of the CC-SN ejecta and the evolution of the main CC-SN observables up to the nebular stage, solving the equations of relativistic radiation hydrodynamics for a self-gravitating fluid which interacts with radiation (describing the ejected material of a CC-SN). Indeed the main features of the `GRRAAL` code are: i) a fully implicit Lagrangian approach to the solution of the system of relativistic radiation hydrodynamics equations, ii) an accurate treatment of radiative transfer coupled to relativistic hydrodynamics, and iii) a self-consistent treatment of the evolution of ejected material taking into account both the gravitational effects of the compact remnant and the heating effects due to decays of radioactive isotopes synthesized during the CC-SN explosion.

We point out that our modelling using both the aforementioned codes, is appropriate only if the emission from the CC-SN is dominated by the expanding ejecta. In the case of SN 2012aw, there could be a contamination from an early interaction with circumstellar matter which may partially affect the observables during the early post-explosion evolution (first ~ 30 days after explosion). Nevertheless, since there is no evidence that such contamination propagates and dominates during most of the evolution, we assume that our modelling can be applied to SN 2012aw, returning a reliable estimate of the physical properties of the progenitor of this event at the explosion (as already done for other CC-SNe with possible contamination from a relatively "weak" interaction like SNe 2007od and 2009bw; see Inserra et al. 2011, 2012). However, in the χ^2 fit we do not include the observational data taken at early phase not only because the behavior of the observables at such phase could be affected by the interaction, but also because of the approximate initial density profile used

in our simulations which does not reproduce accurately the radial profile of the outermost high-velocity shell of the ejecta formed after shock breakout (cf. Pumo & Zampieri 2011).

The explosion epoch (JD = 2456002.5) and distance modulus ($\mu = 29.96$ mag) adopted in this paper (cfr. Sect. 2) were used to fix the explosion epoch and to evaluate the bolometric luminosity of SN 2012aw for comparison with model calculations.

A wide range of semi-analytical models were computed, covering a wide range of masses. In fig. 5 (left upper panel), we show the χ^2 distribution of the computed models. The plot shows that we obtained a quite flat distribution between $\sim 15M_\odot$ and $\sim 28M_\odot$, with the absolute minimum at $\sim 21M_\odot$. Significant minima occur also at $\sim 16M_\odot$ and $\sim 27M_\odot$. In the right upper panel and in the bottom panels of fig. 5, we compare the output of the semi-analytical analysis for the models of $\sim 12M_\odot$, $\sim 16M_\odot$ and $\sim 21M_\odot$. The best agreement with the observational quantitities is reached with the $\sim 21M_\odot$ model, while in the $\sim 12M_\odot$ computed temperatures and velocities are significantly discrepant from observations. The $\sim 21M_\odot$ model was therefore adopted to individuate the parameter space for the `GRRAAL` simulation.

Fig. 6 shows the result of the hydrodynamical simulation. Assuming a ^{56}Ni mass of $\sim 0.07M\odot$ (see Sect. 5), the best fits of the semi-analytic and numerical model are in fair agreement and return values of total (kinetic plus thermal) energy of 1.6-1.7 foe, initial radius of 2.2-3.3 $\times 10^{13}$ cm, and envelope mass of $21 - 23M_\odot$). The values of the modelling parameters reported above are consistent with a scenario where the SN is produced by a relatively massive progenitor having a total mass of $\sim 22.5 - 24.5M_\odot$ at the explosion.

7. Conclusions

We have presented the results of our photometric and spectroscopic campaign of the IIP SN 2012aw. Our photometry maps the SN from the explosion up to the end of the plateau (at Day $\sim$ 125), in th UV-optical-NIR bands; morevoer, two additional epochs were collected in the nebular phase (at Day 286 and Day 333), to get an estimate of the ^{56}Ni mass. Spectroscopic data map the SN evolution from Day 2 to Day 90. Our data allowed us to build a detailed picture of the 2012aw, by deriving all the relevant diagnostics, namely the expansion velocity and the photospheric temperature evolution, and estimating its physical parameters. We adopted the distance modulus ($\mu = 29.96 \pm 0.04$ mag) by averaging the Cepheids (Freedman et al. 2001) and the TRGB (Rizzi et al. 2007) distances, while we estimated the Galactic reddening from Schlegel et al. (1998). The host reddening was evaluated by measuring the Na ID EW on a high-resolution spectrum, obtaining the

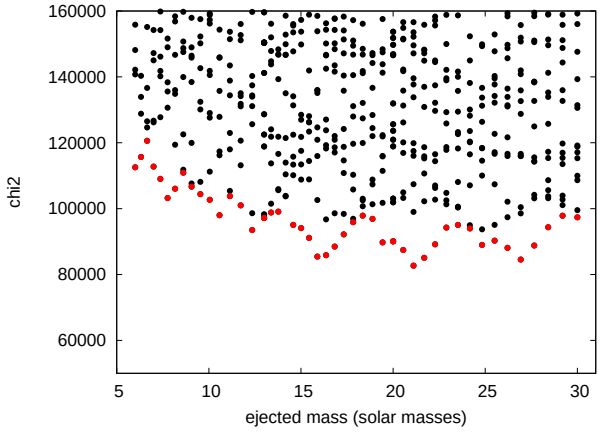
chi2
ejected mass (solar masses)

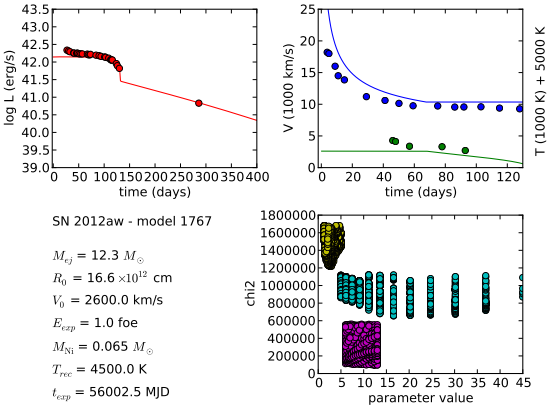
log L (erg/s)
time (days)
V (1000 km/s)
T (1000 K) + 5000 K
SN 2012aw - model 1767
M_{ej} = 12.3 $M_\odot$
R_0 = 16.6 $\times 10^{12}$ cm
V_0 = 2600.0 km/s
E_{exp} = 1.0 foe
$M_{\rm Ni}$ = 0.065 $M_\odot$
T_{rec} = 4500.0 K
t_{exp} = 56002.5 MJD
chi2
parameter value

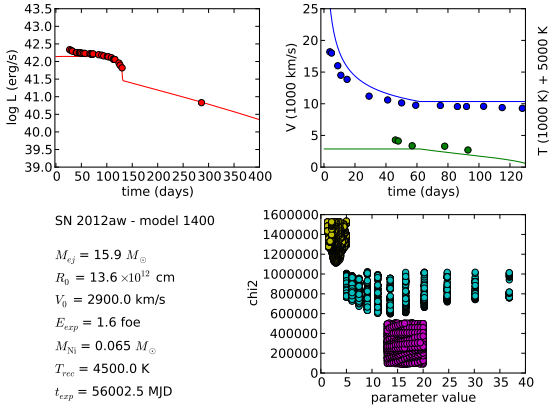
log L (erg/s)
time (days)
V (1000 km/s)
T (1000 K) + 5000 K
SN 2012aw - model 1400
M_{ej} = 15.9 $M_\odot$
R_0 = 13.6 $\times 10^{12}$ cm
V_0 = 2900.0 km/s
E_{exp} = 1.6 foe
$M_{\rm Ni}$ = 0.065 $M_\odot$
T_{rec} = 4500.0 K
t_{exp} = 56002.5 MJD
chi2
parameter value

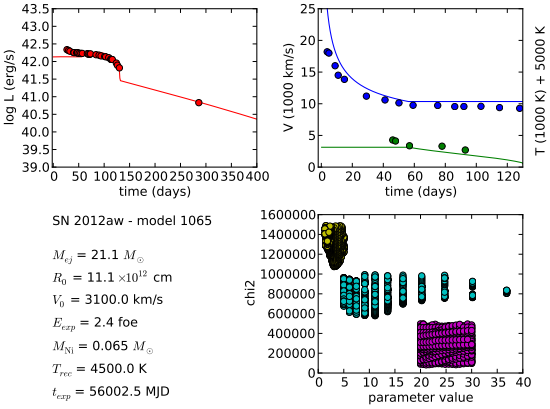
log L (erg/s)
time (days)
V (1000 km/s)
T (1000 K) + 5000 K
SN 2012aw - model 1065
M_{ej} = 21.1 $M_\odot$
R_0 = 11.1 $\times 10^{12}$ cm
V_0 = 3100.0 km/s
E_{exp} = 2.4 foe
$M_{\rm Ni}$ = 0.065 $M_\odot$
T_{rec} = 4500.0 K
t_{exp} = 56002.5 MJD
chi2
parameter value

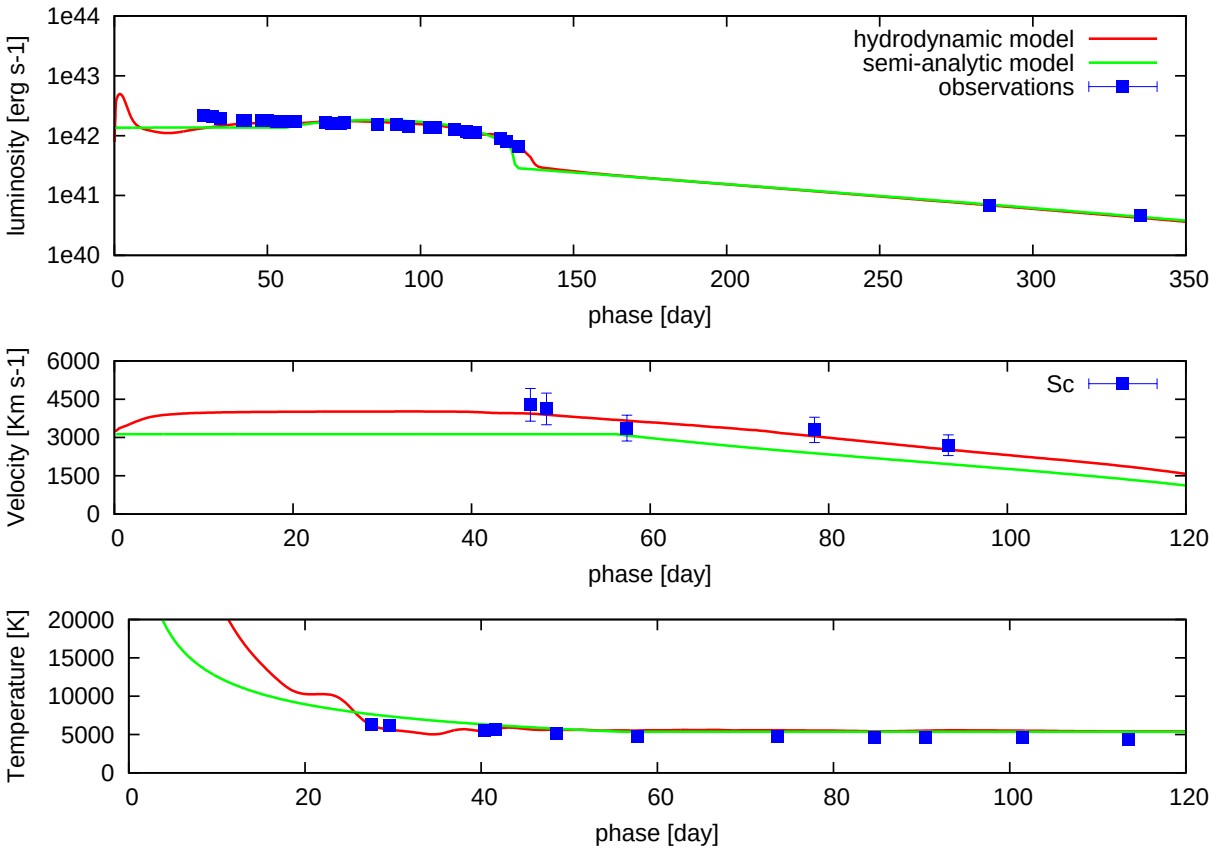

Fig. 6.— Comparison of the evolution of the main observables of SN 2012aw with the best-fit models computed with the semi-analytic code (total energy ~ 1.6 foe, initial radius $\sim 2.2 \times 10^{13}$ cm, envelope mass $\sim 21 M_{\odot}$) and with the GRRAAL code (total energy 1.7 foe, initial radius 3.5×10^{13} cm, envelope mass $22.5 M_{\odot}$). Top, middle, and bottom panels show the bolometric light curve, the photospheric velocity, and the photospheric temperature as a function of time. To better estimate the photosphere velocity from observations, we use the minima of the profile of the Sc II lines.

relatively high $E(B-V) = 0.19$ mag. Our high host galaxy correction is also supported by the photometric calibration of the "end of the plateau" Olivares E. et al. (2010).

With the adopted distance and reddening values, our analysis of the bolometric light curve shows that SN 2012aw has one of the highest luminosities among Type IIP SNe, and consequently a large ejected mass of ^{56}Ni of $0.073 \pm 0.01 M_{\odot}$. The SED shows a general good fit with a single blackbody curve, even if shortward of ~ 4000 Å we observe a higher flux, which could be explained in terms of a higher temperature component. According to Bayless et al. (2013), the observed UV long plateau may indicate a constant temperature, which requires a source of heating. This hypothesis is also supported by the derived photospheric temperature time evolution, which shows a flattening starting from Day ~ 3.

From the collected spectra we measured a fairly large initial expansion velocity, of $\sim 14,000$ Km s^{-1} in the Hα line. After ≈ 50 days from the explosion, they settle on a constant value of ~ 6000 and ~ 5000 Km s^{-1} in the Hα and Hβ lines, respectively. Starting from Day ~ 25, we were able to measure the expansion velocity from the Fe II and Sc II lines, which are known to be better tracers of the photospheric velocities, getting ~ 3000 Km s^{-1}. This behaviour is in agreement with those showed by other luminous Type IIP SN, such as SN 2009bw (Inserra et al. 2012).

We estimated the SN 2012aw physical parameters by means of the hydrodynamical modelling described in Sec.6, which uses the new code GRAAL (Pumo et al. 2010; Pumo & Zampieri 2011), getting the envelope mass $M_{env} \sim 21-23 M_{\odot}$, the radius $R \sim 2.3-3.3 \times 10^{13}$ cm, the energy $E \sim 1.6-1.7$ foe, and an initial $^{56}\mathrm{Ni} = 0.078 M_{\odot}$. We explicitly note that our progenitor mass and the radius estimates are in very good agreement with the independent evolutionary models-based values given by Fraser et al. (2012), who give $M \sim 14 - 26 M_{\odot}$ and $R > 500 R_{\odot} \simeq 7.5^{12}$ cm. Taken at their face values, these estimates indicate a high-mass SN progenitor, with a mass significantly higher than the observational limit of $16.5 \pm 1.5 M_{\odot}$ that rises the "RSG problem" (Smartt et al. 2009), and in agreement with the higher mass limit of $21^{+2}_{-1} M_{\odot}$ given by Walmswell & Eldridge (2012). In the literature is reported that the ejecta masses estimated from the modelling are generally too high to be consistent with the initial masses determined from direct observations of SN progenitors (e.g. Utrobin & Chugai 2009, Maguire et al. 2010). However, our adopted code gives lower ejecta masses, as noted in Jerkstrand et al. (2012).

It is interesting to compare our results with those obtained by Bose et al. (2013), who give an estimate of the explosion energy and the progenitor mass by using the analytical relations given by Litvinova & Nadezhin (1985) and by adopting the radiation hydrodynamical simulations provided by Dessart et al. (2010). Their analysis points toward the energy of explosion in the range $1-2$ foe and the mass of progenitor of about $14-15 M_{\odot}$. It should be

noted that Bose et al. (2013) found several similarities between SN 2012aw with SN 2004et and SN 1999em, on the basis of Utrobin & Chugai (2009) and Utrobin & Chugai (2011) investigations. However, in the same papers the estimated progenitor masses are quite large, of the order of $20 - 25 M_{\odot}$. Moreover, Bose et al. (2013) found some evidence of interaction with the circumstellar medium, which implies a quite large mass loss during the progenitor star lifetime, to reconcile with an initial mass of $14 - 15 M_{\odot}$. Clearly, such differences are due mostly to the different models adopted, and it would be interesting to perform a detailed comparison of the different available codes on the same objects, to check how consistent the results are. [4].

Finally, it should be noted that, as stated by Brown & Woosley (2013): *"the best we can say at the present time is what supernova mass limits might be consistent with observations. The idea of a limiting mass is itself an approximation, since the compactness of the core is not a monotonic function of main sequence mass [...], especially in the interesting range* $20 - 35 M\odot$*"*.

We acknowledge the TriGrid VL project and the INAF-Astronomical Observatory of Padua for the use of computer facilities. M.L.P. acknowledges the financial support from the PRIN-INAF 2009 "Supernovae Variety and Nucleosynthesis Yields" (P.I. S. Benetti).

REFERENCES

Arnett, W. D., Bahcall, J. N., Kirshner, R. P., & Woosley, S. E. 1989, ARA&A, 27, 629

Arnett, W. D., & Fu, A. 1989, ApJ, 340, 396

Barbon, R., Ciatti, F., & Rosino, L. 1979, A&A, 72, 287

Bayless, A. J., Pritchard, T. A., Roming, P. W. A., et al. 2013, ApJ, 764, L13

Beifiori, A., Sarzi, M., Corsini, E. M., et al. 2009, ApJ, 692, 856

Bessell, M. S., & Brett, J. M. 1988, PASP, 100, 1134

Bohlin, R. C., Savage, B. D., & Drake, J. F. 1978, ApJ, 224, 132

[4]A similar experiment was already performed to test how different evolutionary models could determine the star formation histories of resolved stellar populations (the *Coimbra Experiment*, see Skillman & Gallart 2002).

Bose, S., Kumar, B., Sutaria, F., et al. 2013, arXiv:1305.3152

Botticella, M. T., Pastorello, A., Smartt, S. J., et al. 2009, MNRAS, 398, 1041

Botticella, M. T., Smartt, S. J., Kennicutt, R. C., et al. 2012, A&A, 537, A132

Botticella, M. T., Trundle, C., Pastorello, A., et al. 2010, ApJ, 717, L52

Bouchet, P., Danziger, I. J., & Lucy, L. B. 1991, AJ, 102, 1135

Branch, D., Benetti, S., Kasen, D., et al. 2002, ApJ, 566, 1005

Brown, J. M., & Woosley, S. E. 2013, arXiv:1302.6973

Bufano, F., Benetti, S., Turatto, M., et al. 2007, The Multicolored Landscape of Compact Objects and Their Explosive Origins, 924, 271

Cardelli, J. A., Clayton, G. C., & Mathis, J. S. 1989, ApJ, 345, 245

Carpenter, J. M. 2001, AJ, 121, 2851

Ciardullo, R., Feldmeier, J. J., Jacoby, G. H., et al. 2002, ApJ, 577, 31

Clocchiatti, A., Benetti, S., Wheeler, J. C., et al. 1996, AJ, 111, 1286

Coppola, G., Dall'Ora, M., Ripepi, V., et al. 2011, MNRAS, 416, 1056

Dahlen, T., Strolger, L.-G., Riess, A. G., et al. 2012, ApJ, 757, 70

Dessart, L., Livne, E., & Waldman, R. 2010, MNRAS, 408, 827

Ekström, S., Georgy, C., Eggenberger, P., et al. 2012, A&A, 537, A146

Elias-Rosa, N., Van Dyk, S. D., Cuillandre, J.-C., Cenko, S. B., & Filippenko, A. V. 2012, The Astronomer's Telegram, 3991, 1

Elmhamdi, A., Danziger, I. J., Chugai, N., et al. 2003, MNRAS, 338, 939

Fagotti, P., Dimai, A., Quadri, U., et al. 2012, Central Bureau Electronic Telegrams, 3054, 1

Fassia, A., Meikle, W. P. S., Chugai, N., et al. 2001, MNRAS, 325, 907

Ferlet, R., Vidal-Madjar, A., & Gry, C. 1985, ApJ, 298, 838

Filippenko, A. V. 1997, ARA&A, 35, 309

Fraser, M., Maund, J. R., Smartt, S. J., et al. 2012, arXiv:1204.1523

Fraser, M., Maund, J. R., Smartt, S. J., et al. 2012, The Astronomer's Telegram, 3994, 1

Freedman, W. L., Madore, B. F., Gibson, B. K., et al. 2001, ApJ, 553, 47

Gurovich, S., Freeman, K., Jerjen, H., Staveley-Smith, L., & Puerari, I. 2010, AJ, 140, 663

Hägele, G. F., Díaz, Á. I., Cardaci, M. V., Terlevich, E., & Terlevich, R. 2007, MNRAS, 378, 163

Hamuy, M. 2003, ApJ, 582, 905

Hamuy, M., & Pinto, P. A. 2002, ApJ, 566, L63

Harutyunyan, A. H., Pfahler, P., Pastorello, A., et al. 2008, A&A, 488, 383

Henden, A., Krajci, T., & Munari, U. 2012, Information Bulletin on Variable Stars, 6024, 1

Immler, S., & Brown, P. J. 2012, The Astronomer's Telegram, 3995, 1

Inserra, C., Turatto, M., Pastorello, A., et al. 2011, MNRAS, 417, 261

Inserra, C., Turatto, M., Pastorello, A., et al. 2012, MNRAS, 422, 1122

Itoh, R., Ui, T., & Yamanaka, M. 2012, Central Bureau Electronic Telegrams, 3054, 2

Jerkstrand, A., Fransson, C., Maguire, K., et al. 2012, A&A, 546, A28

Jordi, K., Grebel, E. K., & Ammon, K. 2006, A&A, 460, 339

Kasen, D., & Woosley, S. E. 2009, ApJ, 703, 2205

Kochanek, C. S., Khan, R., & Dai, X. 2012, arXiv:1208.4111

Leonard, D. C., Pignata, G., Dessart, L., et al. 2012, The Astronomer's Telegram, 4033, 1

Lenz, D. D., Newberg, J., Rosner, R., Richards, G. T., & Stoughton, C. 1998, ApJS, 119, 121

Limongi, M., & Chieffi, A. 2003, ApJ, 592, 404

Litvinova, I. Y., & Nadezhin, D. K. 1985, Soviet Astronomy Letters, 11, 145

Maguire, K., Di Carlo, E., Smartt, S. J., et al. 2010, MNRAS, 404, 981

Millard, J., Branch, D., Baron, E., et al. 1999, ApJ, 527, 746

Munari, U., Henden, A., Belligoli, R., et al. 2013, New A, 20, 30

Munari, U., Vagnozzi, A., & Castellani, F. 2012, Central Bureau Electronic Telegrams, 3054, 3

Nugent, P., Sullivan, M., Ellis, R., et al. 2006, ApJ, 645, 841

Olivares E., F., Hamuy, M., Pignata, G., et al. 2010, ApJ, 715, 833

Parrent, J., Branch, D., Troxel, M. A., et al. 2007, PASP, 119, 135

Pastorello, A., Pumo, M. L., Navasardyan, H., et al. 2012, A&A, 537, A141

Pastorello, A., Valenti, S., Zampieri, L., et al. 2009, MNRAS, 394, 2266

Poznanski, D., Butler, N., Filippenko, A. V., et al. 2009, ApJ, 694, 1067

Poznanski, D., Nugent, P. E., Ofek, E. O., Gal-Yam, A., & Kasliwal, M. M. 2012, The Astronomer's Telegram, 3996, 1

Poznanski, D., Prochaska, J. X., & Bloom, J. S. 2012, MNRAS, 426, 1465

Pumo, M. L., & Zampieri, L. 2011, ApJ, 741, 41

Pumo, M. L., Zampieri, L., & Turatto, M. 2010, Memorie della Societa Astronomica Italiana Supplementi, 14, 123

Rizzi, L., Tully, R. B., Makarov, D., et al. 2007, ApJ, 661, 815

Sandage, A., & Tammann, G. A. 1987, Carnegie Institution of Washington Publication, Washington: Carnegie Institution, 1987, 2nd ed.

Schlegel, D. J., Finkbeiner, D. P., & Davis, M. 1998, ApJ, 500, 525

Siviero, A., Tomasella, L., Pastorello, A., et al. 2012, Central Bureau Electronic Telegrams, 3054, 4

Skillman, E. D., & Gallart, C. 2002, Observed HR Diagrams and Stellar Evolution, 274, 535

Smartt, S. J. 2009, ARA&A, 47, 63

Smartt, S. J., Eldridge, J. J., Crockett, R. M., & Maund, J. R. 2009, MNRAS, 395, 1409

Springob, C. M., Haynes, M. P., Giovanelli, R., & Kent, B. R. 2005, ApJS, 160, 149

Stockdale, C. J., Ryder, S. D., Van Dyk, S. D., et al. 2012, The Astronomer's Telegram, 4012, 1

Turatto, M., Benetti, S., & Cappellaro, E. 2003, From Twilight to Highlight: The Physics of Supernovae, 200

Utrobin, V. P., & Chugai, N. N. 2009, A&A, 506, 829

Utrobin, V. P., & Chugai, N. N. 2011, A&A, 532, A100

Valenti, S., Fraser, M., Benetti, S., et al. 2011, MNRAS, 416, 3138

Van Dyk, S. D., Cenko, S. B., Poznanski, D., et al. 2012, arXiv:1207.2811

Walmswell, J. J., & Eldridge, J. J. 2012, MNRAS, 419, 2054

Yadav, N., Chakraborti, S., & Ray, A. 2012, The Astronomer's Telegram, 4010, 1

Zampieri, L., Pastorello, A., Turatto, M., et al. 2003, MNRAS, 338, 711

Table 1: Positions and photometry of the selected reference stars. $UBVRI$ and $ugriz$ magnitudes are calibrated with Landolt fields in photometric nights; JHK magnitudes have been taken directly from the 2MASS catalogue. Star IDs are the same for the three systems.

Star ID	$\alpha_{J2000.0}$ (deg)	$\delta_{J2000.0}$ (deg)	U (mag)	B (mag)	V (mag)	R (mag)	I mag
1	160.94117	11.617182		16.384 ± 0.018	15.620 ± 0.006	15.076 ± 0.009	14.694 ± 0.013
2	160.92930	11.647304	15.729 ± 0.008	15.613 ± 0.012	14.853 ± 0.020	14.416 ± 0.020	14.018 ± 0.020
3	160.93780	11.684113	15.221 ± 0.009	15.351 ± 0.040	14.972 ± 0.028	14.706 ± 0.026	14.450 ± 0.012
4	160.92599	11.743191		17.116 ± 0.012	15.821 ± 0.005	14.952 ± 0.006	14.104 ± 0.030
5	160.88154	11.620989		14.992 ± 0.026	13.932 ± 0.038	13.248 ± 0.028	12.717 ± 0.034
6	160.91103	11.5839790		15.551 ± 0.018	14.669 ± 0.020	14.145 ± 0.012	13.670 ± 0.002
7	161.06876	11.576971		15.706 ± 0.009	14.873 ± 0.034	14.334 ± 0.019	13.949 ± 0.004
8	161.11392	11.571762		14.249 ± 0.022	13.516 ± 0.029	13.088 ± 0.026	12.718 ± 0.025

Star ID	$\alpha_{J2000.0}$ (deg)	$\delta_{J2000.0}$ (deg)	u (mag)	g (mag)	r (mag)	i (mag)	z mag
1	160.94117	11.617182		15.967 ± 0.024	15.372 ± 0.021	15.168 ± 0.015	15.105 ± 0.018
2	160.92930	11.647304	16.612 ± 0.044	15.244 ± 0.018	14.653 ± 0.016	14.433 ± 0.008	14.312 ± 0.012
3	160.93780	11.684113	16.092 ± 0.029	15.108 ± 0.018	14.883 ± 0.016	14.823 ± 0.012	14.830 ± 0.021

Star ID	$\alpha_{J2000.0}$ (deg)	$\delta_{J2000.0}$ (deg)	J (mag)	H (mag)	K (mag)
2	160.92930	11.647304	13.380 ± 0.027	13.025 ± 0.026	12.914 ± 0.034
4	160.94117	11.617182	13.163 ± 0.026	12.476 ± 0.024	12.347 ± 0.031
9	160.93780	11.684113	12.816 ± 0.024	12.218 ± 0.024	12.001 ± 0.021
10	160.91448	11.738809	10.233 ± 0.027	9.741 ± 0.026	9.554 ± 0.027

Table 2: Log of $UBVRI$ photometric observations of SN 2012aw. See text for the details on the individuals instruments.

Date	JD (2400000+)	Phase[a] (days)	U (mag)	B (mag)	V (mag)	R (mag)	I (mag)	Source[b]
17/03/2012	56004.41	1.9		13.79 ± 0.01	13.86 ± 0.01	13.82 ± 0.01	13.72 ± 0.01	1
18/03/2012	56005.57	3.1		13.52 ± 0.05	13.68 ± 0.05	13.53 ± 0.03	13.53 ± 0.01	12
19/03/2012	56006.71	4.2		13.47 ± 0.12	13.59 ± 0.11	13.40 ± 0.09	13.39 ± 0.07	12
19/03/2012	56006.41	3.9		13.60 ± 0.01	13.58 ± 0.01	13.43 ± 0.01	13.31 ± 0.01	1
19/03/2012	56006.44	3.9		13.54 ± 0.08	13.56 ± 0.07	13.35 ± 0.05	13.41 ± 0.05	2
20/03/2012	56007.57	5.1		13.47 ± 0.11	13.52 ± 0.10	13.29 ± 0.08	13.28 ± 0.06	12
20/03/2012	56007.31	4.8		13.53 ± 0.06	13.52 ± 0.06	13.38 ± 0.05	13.39 ± 0.05	2
21/03/2012	56008.57	6.1		13.38 ± 0.05	13.39 ± 0.05	13.22 ± 0.03	13.20 ± 0.04	12
21/03/2012	56008.31	5.8		13.41 ± 0.05	13.44 ± 0.05	13.27 ± 0.06	13.22 ± 0.05	2
22/03/2012	56009.58	7.1		13.42 ± 0.02	13.38 ± 0.02	13.11 ± 0.04	13.13 ± 0.03	12
22/03/2012	56009.31	6.8		13.42 ± 0.04	13.36 ± 0.04	13.19 ± 0.04	13.16 ± 0.02	2
23/03/2012	56010.54	8.0		13.36 ± 0.02	13.34 ± 0.02	13.11 ± 0.03	13.11 ± 0.02	12
23/03/2012	56010.35	7.8		13.43 ± 0.02	13.34 ± 0.02	13.18 ± 0.03	13.11 ± 0.01	2
23/03/2012	56010.35	7.8	12.50 ± 0.04	13.35 ± 0.02	13.30 ± 0.02	13.10 ± 0.01	13.07 ± 0.03	3
23/03/2012	56010.36	7.9		13.39 ± 0.03	13.30 ± 0.03	13.12 ± 0.01	13.12 ± 0.01	2
24/03/2012	56011.54	9.0		13.38 ± 0.03	13.28 ± 0.03	13.11 ± 0.02	13.07 ± 0.02	12
24/03/2012	56011.36	8.9	12.55 ± 0.08	13.32 ± 0.03	13.29 ± 0.02	13.12 ± 0.02	13.06 ± 0.03	3
26/03/2012	56013.36	10.9	12.74 ± 0.07	13.43 ± 0.06				5
26/03/2012	56013.39	10.9			13.33 ± 0.03	13.16 ± 0.04	13.08 ± 0.03	2
27/03/2012	56014.44	11.9		13.43 ± 0.03	13.31 ± 0.03			2
28/03/2012	56015.53	13.0		13.51 ± 0.04	13.35 ± 0.03	13.13 ± 0.02	13.07 ± 0.02	12
28/03/2012	56015.39	12.9	12.84 ± 0.06	13.50 ± 0.02	13.35 ± 0.02	13.12 ± 0.02	13.07 ± 0.05	5
29/03/2012	56016.51	14.0		13.48 ± 0.02	13.35 ± 0.02	13.11 ± 0.02	13.03 ± 0.04	12
29/03/2012	56016.37	13.9		13.46 ± 0.03	13.30 ± 0.03	13.12 ± 0.03	13.01 ± 0.01	2
30/03/2012	56017.57	15.1		13.61 ± 0.09	13.34 ± 0.08	13.14 ± 0.03	12.98 ± 0.03	12
30/03/2012	56017.37	14.9				13.08 ± 0.02	13.02 ± 0.03	12
31/03/2012	56018.43	15.9		13.53 ± 0.02	13.29 ± 0.02	13.13 ± 0.03	12.98 ± 0.02	2
02/04/2012	56020.32	17.8		13.58 ± 0.07	13.34 ± 0.06	13.13 ± 0.05	12.92 ± 0.03	2
11/04/2012	56029.53	27.0			13.37 ± 0.06	13.06 ± 0.08	12.90 ± 0.03	12
14/04/2012	56032.60	30.1			13.40 ± 0.01	13.05 ± 0.01	12.90 ± 0.05	12
17/04/2012	56035.55	33.0			13.44 ± 0.02	13.09 ± 0.01	12.88 ± 0.01	12
24/04/2012	56042.43	39.9		14.41 ± 0.03	13.42 ± 0.02	13.13 ± 0.03	12.86 ± 0.02	2
25/04/2012	56043.40	40.9		14.41 ± 0.04	13.44 ± 0.04	13.08 ± 0.03	12.84 ± 0.04	2
25/04/2012	56043.49	41.0		14.43 ± 0.01	13.45 ± 0.01	13.06 ± 0.03	12.91 ± 0.04	7
30/04/2012	56048.55	46.0	15.43 ± 0.02	14.45 ± 0.02	13.46 ± 0.02	13.07 ± 0.02	12.84 ± 0.02	6
02/05/2012	56049.94	47.4			13.50 ± 0.02	13.05 ± 0.03	12.80 ± 0.04	12
03/05/2012	56050.57	48.1		14.54 ± 0.04	13.46 ± 0.04	13.07 ± 0.04	12.79 ± 0.03	12
06/05/2012	56053.40	50.9	15.70 ± 0.03	14.72 ± 0.02	13.54 ± 0.02	13.07 ± 0.04	12.82 ± 0.05	13
09/05/2012	56056.61	54.1			13.53 ± 0.02	13.08 ± 0.03	12.81 ± 0.02	12
12/05/2012	56059.65	57.2		14.71 ± 0.08	13.53 ± 0.08	13.10 ± 0.04	12.80 ± 0.01	12
21/05/2012	56069.55	67.0		15.10 ± 0.06	13.56 ± 0.05	13.02 ± 0.03	12.76 ± 0.03	12
23/05/2012	56071.57	69.1			13.59 ± 0.03	13.02 ± 0.04	12.90 ± 0.04	12
26/05/2012	56074.38	71.9	16.56 ± 0.05	14.97 ± 0.01	13.60 ± 0.01	13.08 ± 0.02	12.83 ± 0.02	7
27/05/2012	56075.61	73.1			13.59 ± 0.02	13.02 ± 0.03	12.75 ± 0.03	12
07/06/2012	56086.55	84.0			13.64 ± 0.01	13.11 ± 0.01		12
13/06/2012	56092.51	90.0			13.67 ± 0.03	13.11 ± 0.03		12
17/06/2012	56096.41	93.9	17.17 ± 0.06	15.19 ± 0.02	13.75 ± 0.02	13.17 ± 0.01	12.88 ± 0.01	7
24/06/2012	56103.53	101.0			13.82 ± 0.04	13.18 ± 0.05	12.88 ± 0.04	12
26/06/2012	56105.40	102.9		15.45 ± 0.04	13.88 ± 0.02	13.21 ± 0.04	12.85 ± 0.06	13
02/07/2012	56111.48	109.0		15.31 ± 0.12	13.90 ± 0.11	13.29 ± 0.05	12.95 ± 0.03	12
06/07/2012	56115.49	113.0		15.45 ± 0.04	14.01 ± 0.03	13.37 ± 0.05	13.08 ± 0.06	12
07/07/2012	56116.40	113.9	17.62 ± 0.05	15.47 ± 0.03	14.03 ± 0.03	13.40 ± 0.02	13.11 ± 0.02	7
08/07/2012	56117.48	115.0		15.49 ± 0.11	14.02 ± 0.10	13.40 ± 0.02	13.12 ± 0.02	12
09/07/2012	56118.49	116.0		15.52 ± 0.05	14.05 ± 0.05	13.37 ± 0.03	13.08 ± 0.02	12
17/07/2012	56126.48	123.0		15.87 ± 0.07	14.32 ± 0.03	13.63 ± 0.03	13.28 ± 0.03	12
19/07/2012	56128.48	126.0		15.92 ± 0.12	14.46 ± 0.11			12
20/07/2012	56129.48	127.0				13.88 ± 0.04	13.57 ± 0.05	12
23/07/2012	56132.47	130.0			14.67 ± 0.01	13.88 ± 0.02		12
26/12/2013	56288.70	286.2		18.55 ± 0.02	17.37 ± 0.02	16.36 ± 0.04	15.90 ± 0.03	7
11/02/2013	56335.63	333.1	20.34 ± 0.10	18.98 ± 0.03	17.80 ± 0.02	16.85 ± 0.01	16.32 ± 0.02	13

Table 3: Log of *ugriz* photometric observations of SN 2012aw. See text for the details on the individual instruments.

Date	JD (2400000+)	Phase[a] (days)	u (mag)	g (mag)	r (mag)	i (mag)	z (mag)	Source[b]
18/03/2012	56005.57	3.1		13.57 ± 0.04	13.68 ± 0.03	13.87 ± 0.02	14.00 ± 0.02	12
19/03/2012	56006.58	4.1		13.46 ± 0.03	13.57 ± 0.02	13.73 ± 0.01	13.84 ± 0.01	12
20/03/2012	56007.57	5.1		13.50 ± 0.04	13.46 ± 0.03	13.62 ± 0.01	13.75 ± 0.02	12
21/03/2012	56008.57	6.1	13.34 ± 0.11	13.40 ± 0.03	13.38 ± 0.02	13.54 ± 0.02	13.67 ± 0.02	12
22/03/2012	56009.58	7.1		13.38 ± 0.03	13.32 ± 0.02	13.49 ± 0.01	13.62 ± 0.02	12
23/03/2012	56010.54	8.0		13.33 ± 0.02	13.31 ± 0.02	13.47 ± 0.01	13.58 ± 0.02	12
23/03/2012	56010.36	7.9	13.29 ± 0.04	13.26 ± 0.03	13.30 ± 0.02	13.43 ± 0.01	13.52 ± 0.01	2
24/03/2012	56011.54	9.0		13.33 ± 0.03	13.28 ± 0.03	13.41 ± 0.01	13.54 ± 0.02	12
25/03/2012	56012.06	9.6		13.30 ± 0.12	13.24 ± 0.13	13.45 ± 0.04	13.54 ± 0.07	10
26/03/2012	56013.49	11.0	13.55 ± 0.14	13.27 ± 0.02	13.26 ± 0.01	13.40 ± 0.02	13.49 ± 0.02	4
28/03/2012	56015.53	13.0		13.38 ± 0.05	13.29 ± 0.05	13.38 ± 0.01	13.47 ± 0.02	12
29/03/2012	56016.51	14.0		13.37 ± 0.04	13.27 ± 0.03	13.40 ± 0.02	13.50 ± 0.02	12
30/03/2012	56017.37	14.9		13.34 ± 0.11	13.32 ± 0.10	13.37 ± 0.03	13.43 ± 0.02	12
06/04/2012	56024.41	21.9	14.39 ± 0.06	13.42 ± 0.02	13.18 ± 0.02	13.26 ± 0.03	13.28 ± 0.01	4
11/04/2012	56029.53	27.0			13.21 ± 0.01	13.28 ± 0.01	13.34 ± 0.01	12
14/04/2012	56032.60	30.1			13.24 ± 0.02	13.29 ± 0.02	13.27 ± 0.03	12
16/04/2012	56034.56	32.1		13.76 ± 0.04	13.21 ± 0.04	13.26 ± 0.01		4
17/04/2012	56035.55	33.0			13.25 ± 0.02	13.31 ± 0.03	13.26 ± 0.01	12
21/04/2012	56039.41	36.9	16.18 ± 0.08	13.82 ± 0.01	13.25 ± 0.01	13.27 ± 0.02	13.24 ± 0.01	4
09/05/2012	56056.61	54.1			13.27 ± 0.02	13.23 ± 0.02	13.14 ± 0.02	12
14/05/2012	56061.58	59.1		14.11 ± 0.03	13.26 ± 0.03	13.21 ± 0.02	13.12 ± 0.01	12
21/05/2012	56069.55	67.0			13.27 ± 0.02	13.22 ± 0.02	13.04 ± 0.04	12
23/05/2012	56071.57	69.1			13.30 ± 0.01	13.22 ± 0.01		12
26/05/2012	56074.43	71.9	17.67 ± 0.16	14.22 ± 0.02	13.27 ± 0.02	13.19 ± 0.01	13.10 ± 0.01	4
27/05/2012	56075.61	73.1			13.27 ± 0.02		13.11 ± 0.02	12
31/05/2012	56079.41	76.9	17.90 ± 0.12	14.22 ± 0.03	13.30 ± 0.02	13.20 ± 0.02	13.11 ± 0.02	4
01/06/2012	56080.41	77.9	17.84 ± 0.10	14.26 ± 0.03	13.27 ± 0.03	13.21 ± 0.02	13.09 ± 0.02	4
07/06/2012	56086.55	84.0			13.29 ± 0.03	13.29 ± 0.03	13.21 ± 0.06	12
24/06/2012	56103.53	101.0			13.42 ± 0.02	13.36 ± 0.02	13.23 ± 0.02	12
07/07/2012	56116.48	114.0			13.62 ± 0.02	13.54 ± 0.02	13.36 ± 0.01	12

[a] JD - 2450002.5

[b] 2 = Asiago Schmidt Telescope; 4=RATCAM; 10 = Faulkes North; 12 = PROMPT.

Table 4: Log of NIR observations of the SN 2012aw. See text for the details on the individual instruments.

Date	JD (2400000+)	Phase[a] (days)	J (mag)	H (mag)	K (mag)	Source[b]
23/03/2012	56010.07	7.6	13.00 ± 0.06	12.95 ± 0.06	12.66 ± 0.06	9
24/03/2012	56011.09	8.6	13.04 ± 0.04	12.87 ± 0.04	12.71 ± 0.07	9
25/03/2012	56012.12	9.6	12.90 ± 0.04	12.78 ± 0.04	12.52 ± 0.04	9
29/03/2012	56016.68	14.2	12.82 ± 0.10	12.63 ± 0.07	12.45 ± 0.06	8
01/04/2012	56019.07	16.6	12.80 ± 0.04	12.62 ± 0.04	12.56 ± 0.04	9
04/04/2012	56022.08	19.6	12.74 ± 0.03	12.57 ± 0.03	12.42 ± 0.04	9
07/04/2012	56025.07	22.6		12.55 ± 0.08	12.35 ± 0.04	9
13/04/2012	56031.37	28.9	12.56 ± 0.07	12.39 ± 0.08		11
17/04/2012	56035.01	32.5	12.54 ± 0.05	12.34 ± 0.05	12.26 ± 0.04	9
22/04/2012	56040.38	37.9			11.96 ± 0.17	11
24/04/2012	56042.12	39.6	12.49 ± 0.09	12.34 ± 0.09	12.14 ± 0.09	9
02/05/2012	56049.99	47.5	12.41 ± 0.04	12.21 ± 0.04	12.08 ± 0.06	9
04/05/2012	56052.42	49.9	12.34 ± 0.04	12.03 ± 0.06		11
15/05/2012	56063.41	60.9	12.49 ± 0.04	12.74 ± 0.07		11
06/06/2012	56085.40	82.9	12.31 ± 0.02	12.18 ± 0.06		11
10/06/2012	56088.41	85.9	12.34 ± 0.04	12.12 ± 0.04	11.97 ± 0.11	11
17/06/2012	56096.44	93.9	12.42 ± 0.03	12.23 ± 0.06	12.04 ± 0.01	11

[a] JD - 2450002.5

[b] 8 = NICS; 9= REM; 11 = TCS.

Table 5: Log of the spectroscopic observations. For each spectrum, we list the UT observation date, the JD, the epoch from the explosion, the wavelength range, the dispersion and the instrument.

Date dd/mm/yyyy	JD 240000+	Epoch (days)	Range Å	Dispersion Å mm^{-1}	Instrument
17/03/2012	56004.X	1.X	3300 − 7800	169	BC@Asiago1.2m
19/03/2012	56004.X	1.X	3300 − 7800	169	BC@Asiago1.2m
19/03/2012	$XXXXXXX$	$XX.X$	3200 − 9100	220	ALFOSC@NOT
20/03/2012	56004.X	1.X	3300 − 7800	169	BC@Asiago1.2m
20/03/2012	56008.4	5.9	3000 − 8400	187	LRS@TNG
20/03/2012	56008.4	5.9	4500 − 10000	193	LRS@TNG
20/03/2012	56004.X	1.X	3300 − 7800	169	BC@Asiago1.2m
21/03/2012	56004.X	1.X	3300 − 7800	169	BC@Asiago1.2m
21/03/2012	56004.X	1.X	4600 − 7900	61	SARG@TNG
22/03/2012	56004.X	1.X	3300 − 7800	169	BC@Asiago1.2m
23/03/2012	56004.X	1.X	3300 − 7800	169	BC@Asiago1.2m
24/03/2012	5600$X.X$	$X.X$	3200 − 7000	185	CAFOS@CAHA
25/03/2012	56004.X	1.X	3300 − 7800	169	BC@Asiago1.2m
26/03/2012	5600$X.X$	$XX.X$	5000 − 11000	191	AFOSC@Ekar1.8m
26/03/2012	5600$X.X$	$XX.X$	3500 − 7700	292	AFOSC@Ekar1.8m
27/03/2012	5600$X.X$	$XX.X$	3500 − 7700	292	AFOSC@Ekar1.8m
28/03/2012	5600$X.X$	$XX.X$	3500 − 7700	292	AFOSC@Ekar1.8m
29/03/2012	56004.X	1.X	3300 − 7800	169	BC@Asiago1.2m
29/03/2012	56004.X	1.X	5000 − 10100	95	SARG@TNG
30/03/2012	560$XX.X$	$XX.X$	9000 − 14500	297	NICS@TNG
30/03/2012	560$XX.X$	$XX.X$	14000 − 25000	605	NICS@TNG
30/03/2012	$XXXXXXX$	$XX.X$	3200 − 9100	220	ALFOSC@NOT
31/03/2012	560$XX.X$	$X1.X$	3300 − 7800	169	BC@Asiago1.2m
31/03/2012	560$XX.X$	$XX.X$	3500 − 5200	64	ISIS@WHT
31/03/2012	560$XX.X$	$XX.X$	5400 − 9500	120	ISIS@WHT
02/04/2012	560$XX.X$	$X1.X$	3300 − 7800	169	BC@Asiago1.2m
08/04/2012	56008.4	5.9	3000 − 8400	187	LRS@TNG
08/04/2012	56008.4	5.9	4500 − 10000	193	LRS@TNG
08/04/2012	$XXXXXXX$	$XX.X$	8000 − 25000	XXX	FIRE@Magellan
11/04/2012	$XXXXXXX$	$XX.X$	8000 − 25000	XXX	FIRE@Magellan
13/04/2012	$XXXXXXX$	$XX.X$	3700 − 9300	185	EFOSC@NTT
25/04/2012	$XXXXXXX$	$XX.X$	3200 − 9100	220	ALFOSC@NOT
29/04/2012	$XXXXXXX$	$XX.X$	8000 − 25000	XXX	FIRE@Magellan
01/05/2012	$XXXXXXX$	$XX.X$	3700 − 9300	185	EFOSC@NTT
07/05/2012	$XXXXXXX$	$XX.X$	8000 − 25000	XXX	FIRE@Magellan
11/05/2012	$XXXXXXX$	$XX.X$	3200 − 9100	220	ALFOSC@NOT
01/06/2012	$XXXXXXX$	$XX.X$	3200 − 9100	220	ALFOSC@NOT
16/06/2012	560$XX.X$	$X1.X$	3300 − 7800	169	BC@Asiago1.2m

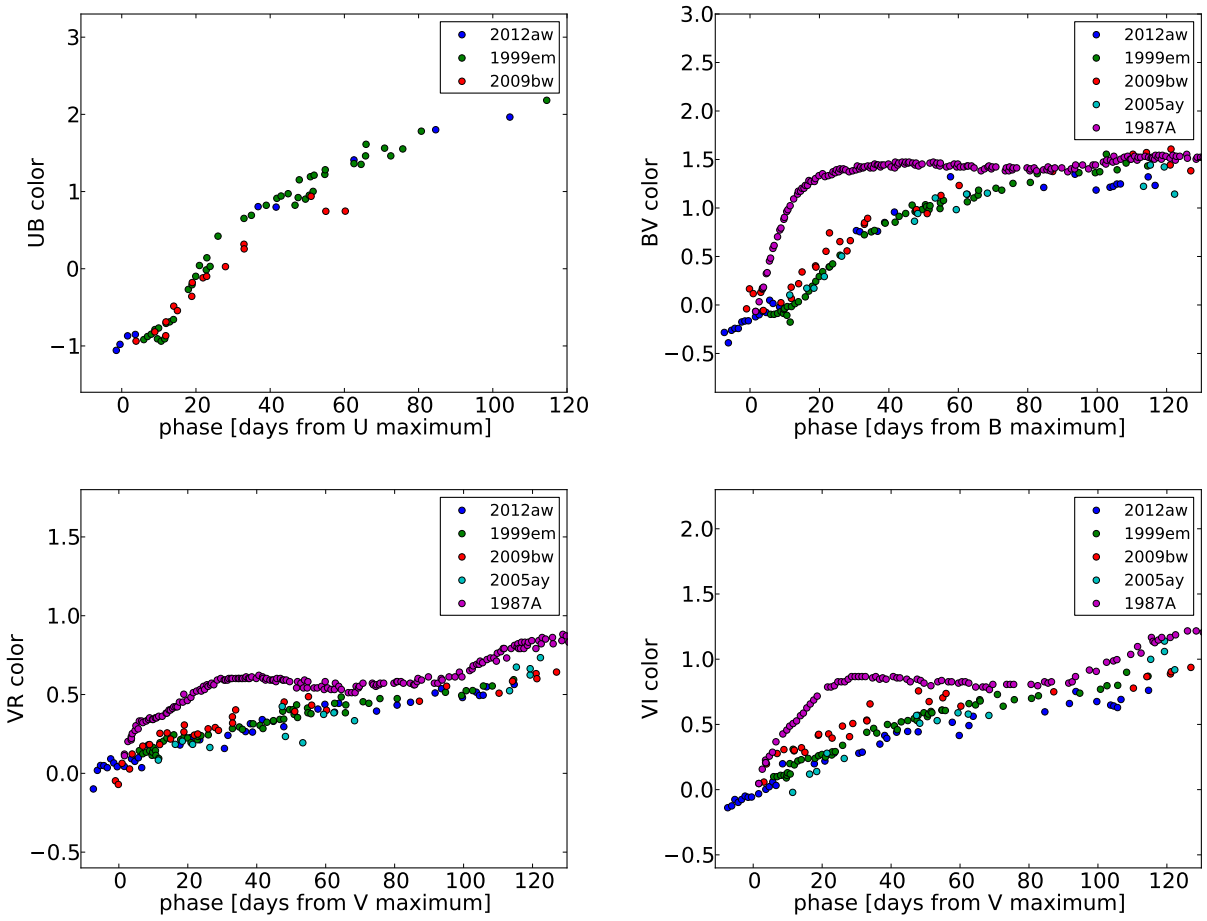

Fig. 7.— Dereddend colour evolution of SN 2012aw in the $UBVRI$ system. Individual panels show the comparisons with other type IIP literature.

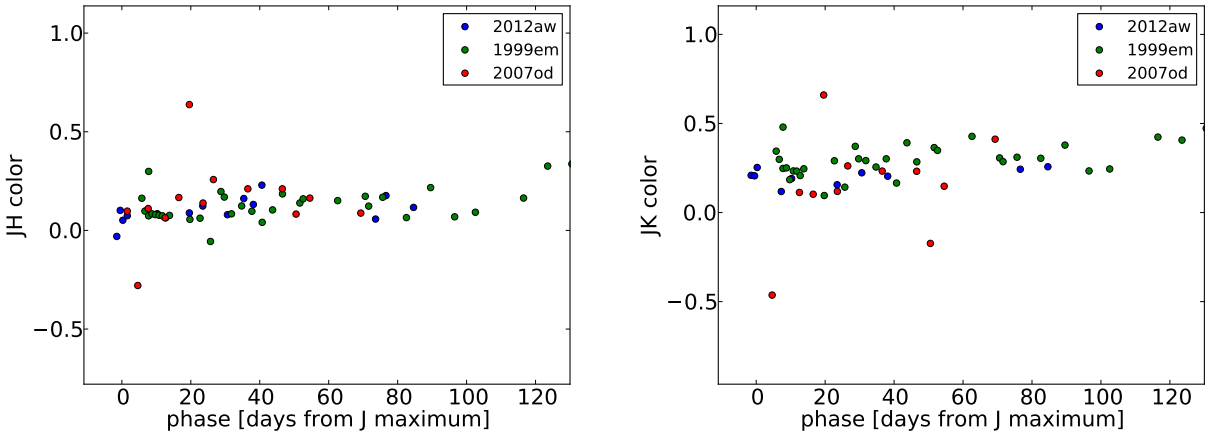

Fig. 8.— $(J-H)$ and $(J-K)$ colour evolution of SN 2012aw, compared with SN 1999em and SN 2007od. Individual colour curves have been dereddened.

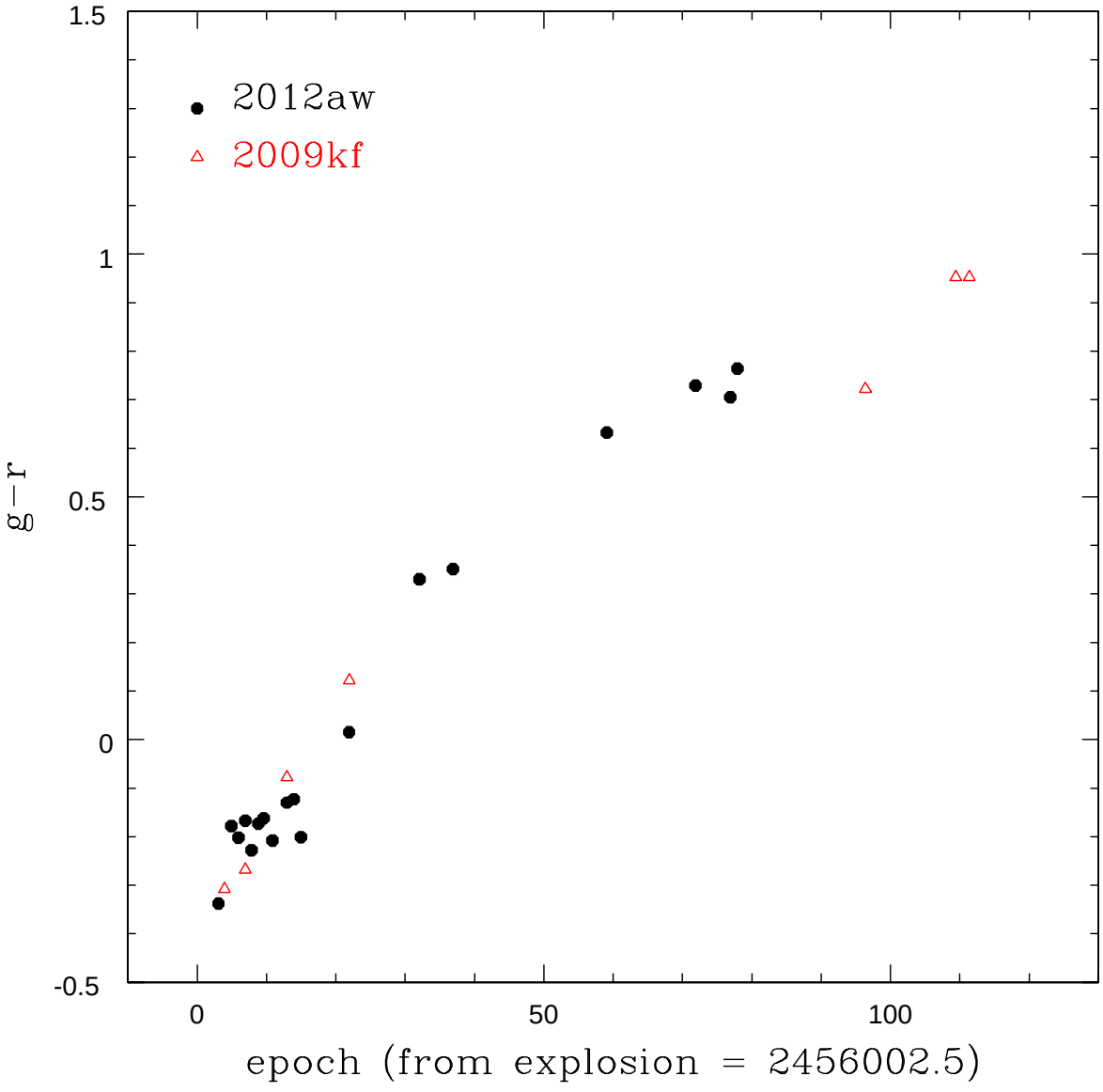

Fig. 9.— Dereddened $(g-r)$ colour curve of SN 2012aw, compared with SN 2009kf.

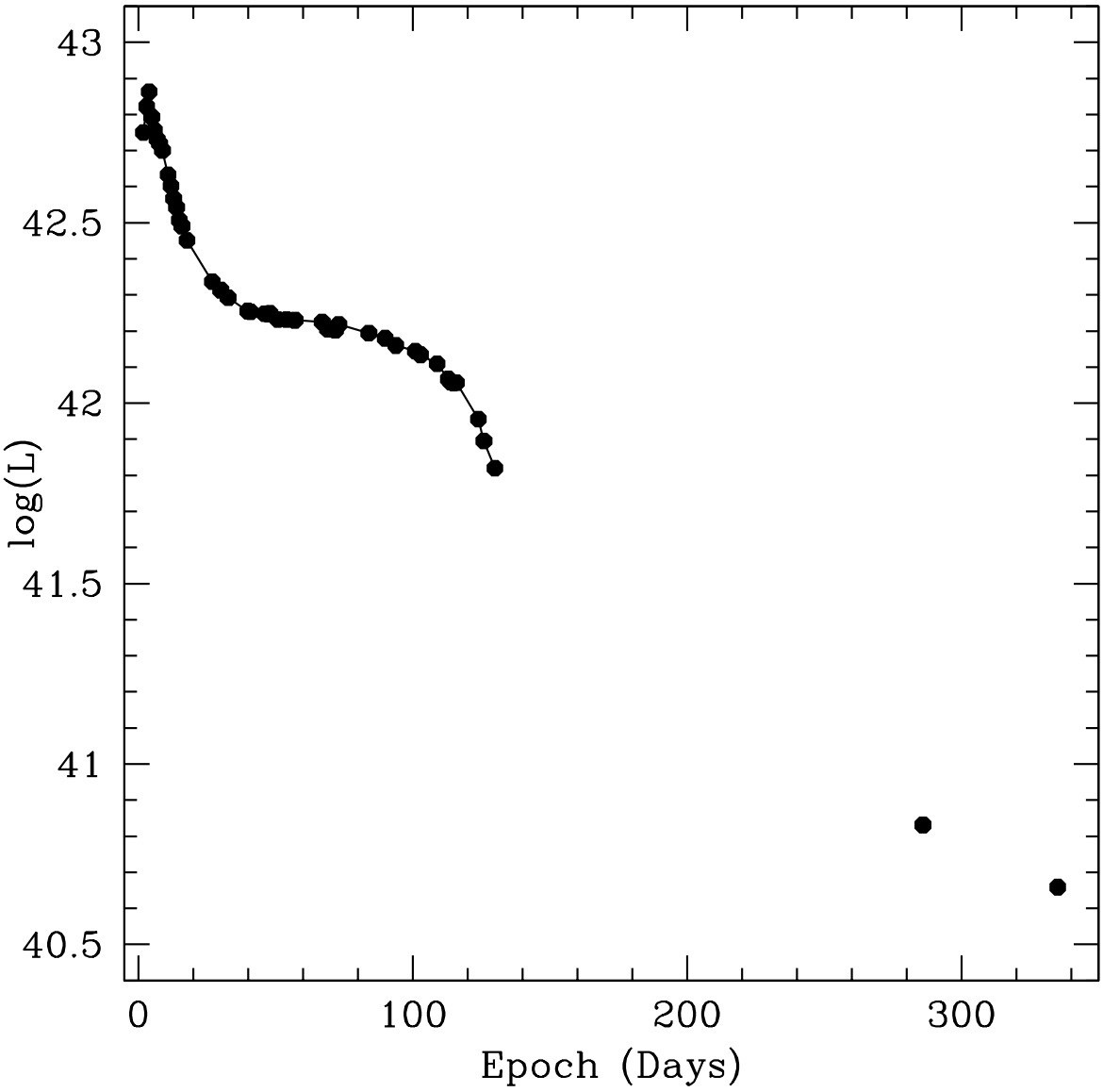

Fig. 10.— UVOIR bolometric light curve of SN 2012aw. The bolometric luminosity was obtained from a full set of Swift$ubw2$, $uvw1$, Johnson-Cousins $UBVRI$ and near-infrared JHK measurements, following the procedure described in the text.

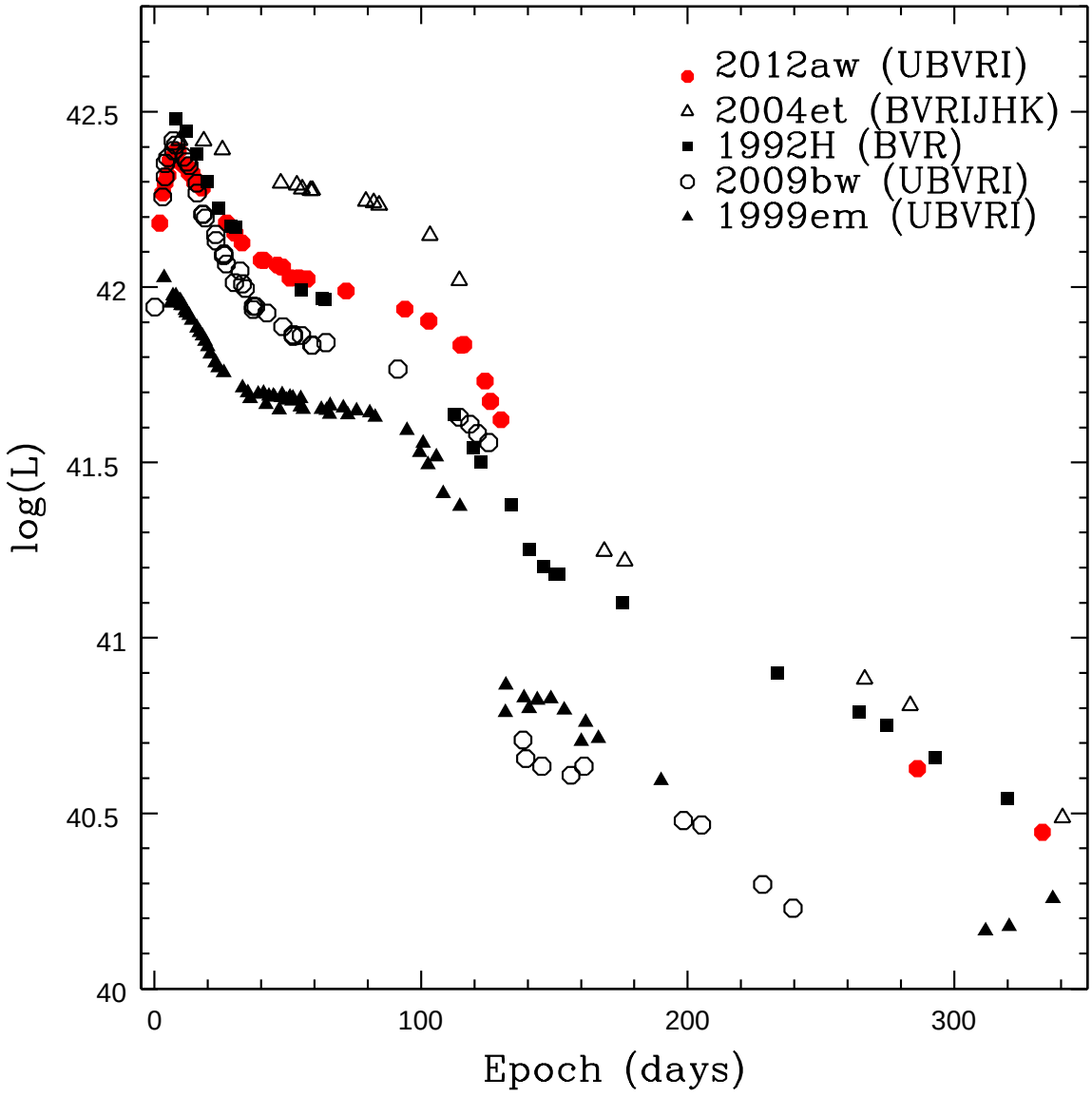

Fig. 11.— $UBVRI$ Pseudo-bolometric light curve of SN 2012aw. The light curve is compared with other literature IIP supernovae.

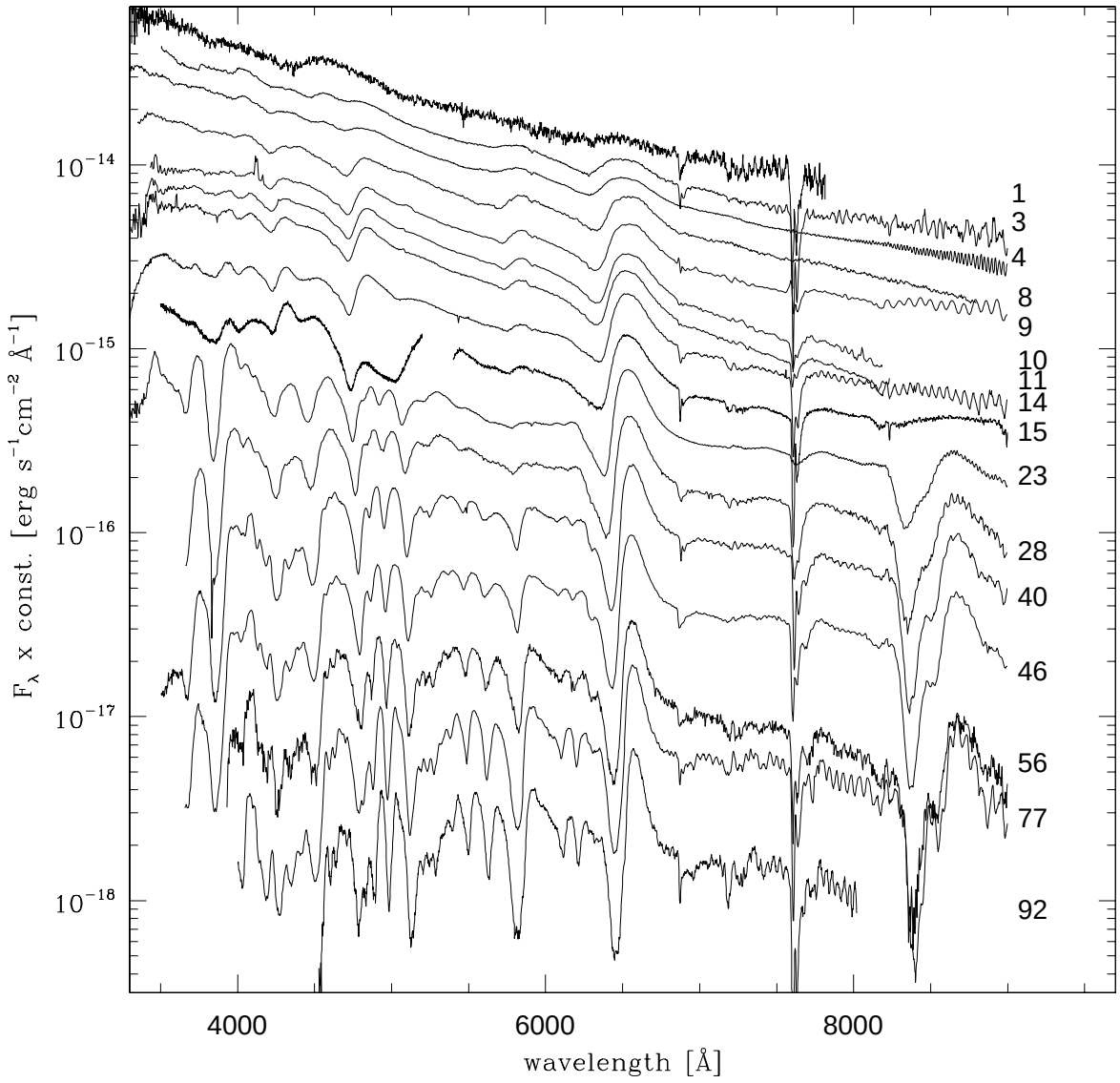
10^{-14}
10^{-15}
10^{-16}
10^{-17}
10^{-18}
F_λ x const. [erg s^{-1}cm^{-2} Å^{-1}]
4000
6000
8000
wavelength [Å]
1
3
4
8
9
10
11
14
15
23
28
40
46
56
77
92

Fig. 12.—

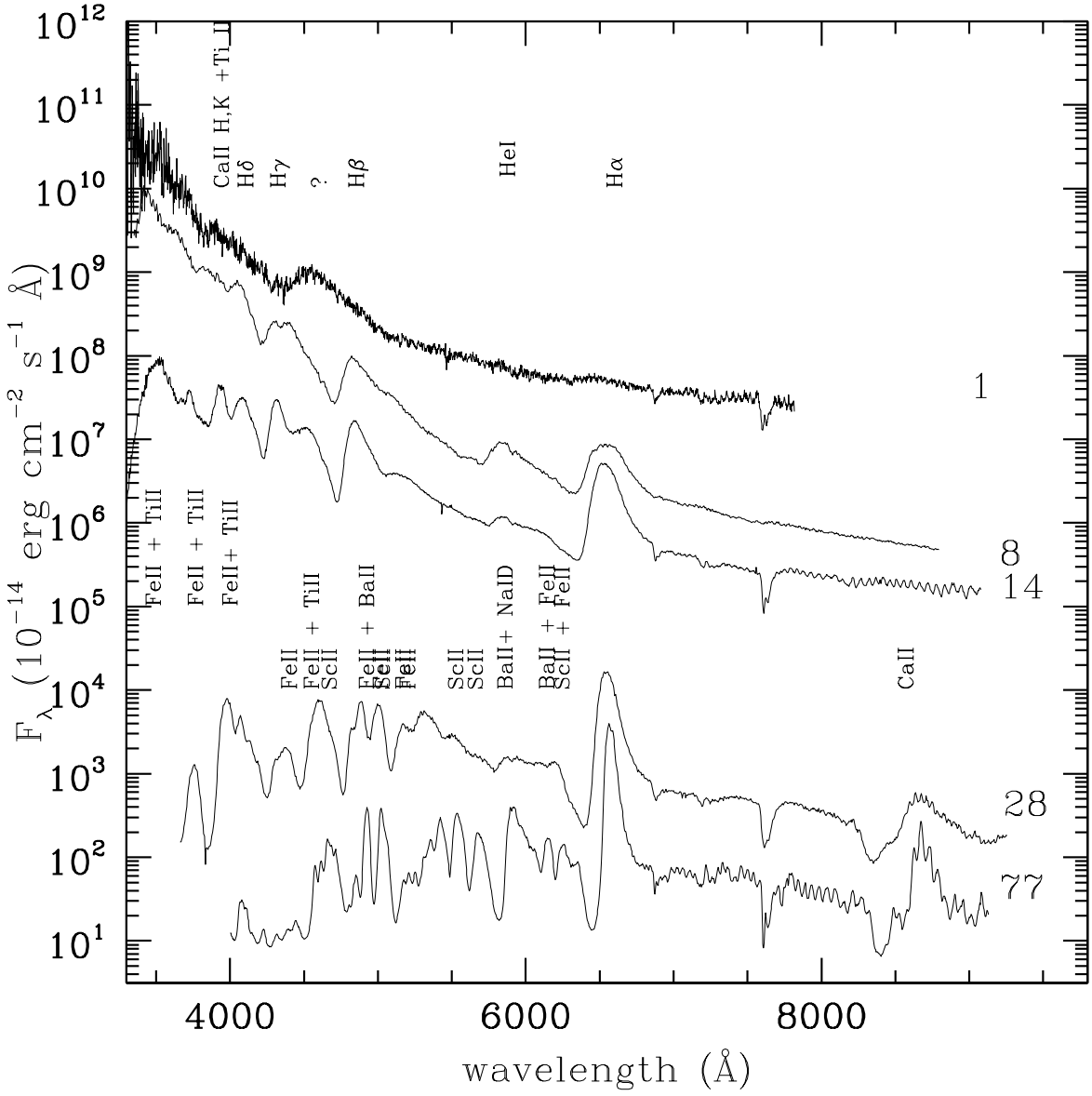
CaII H,K +Ti_II
Hδ
Hγ
?
Hβ
HeI
Hα
FeII + TiII
FeII + TiII
FeII+ TiII
FeII + TiII
FeII + BaII
ScII
ScII
BaII+ NaID
BaII + FeII
ScII + FeII
CaII
1
8
14
28
77
$F_\lambda (10^{-14}$ erg cm^{-2} s^{-1} Å)
wavelength (Å)

Fig. 13.—

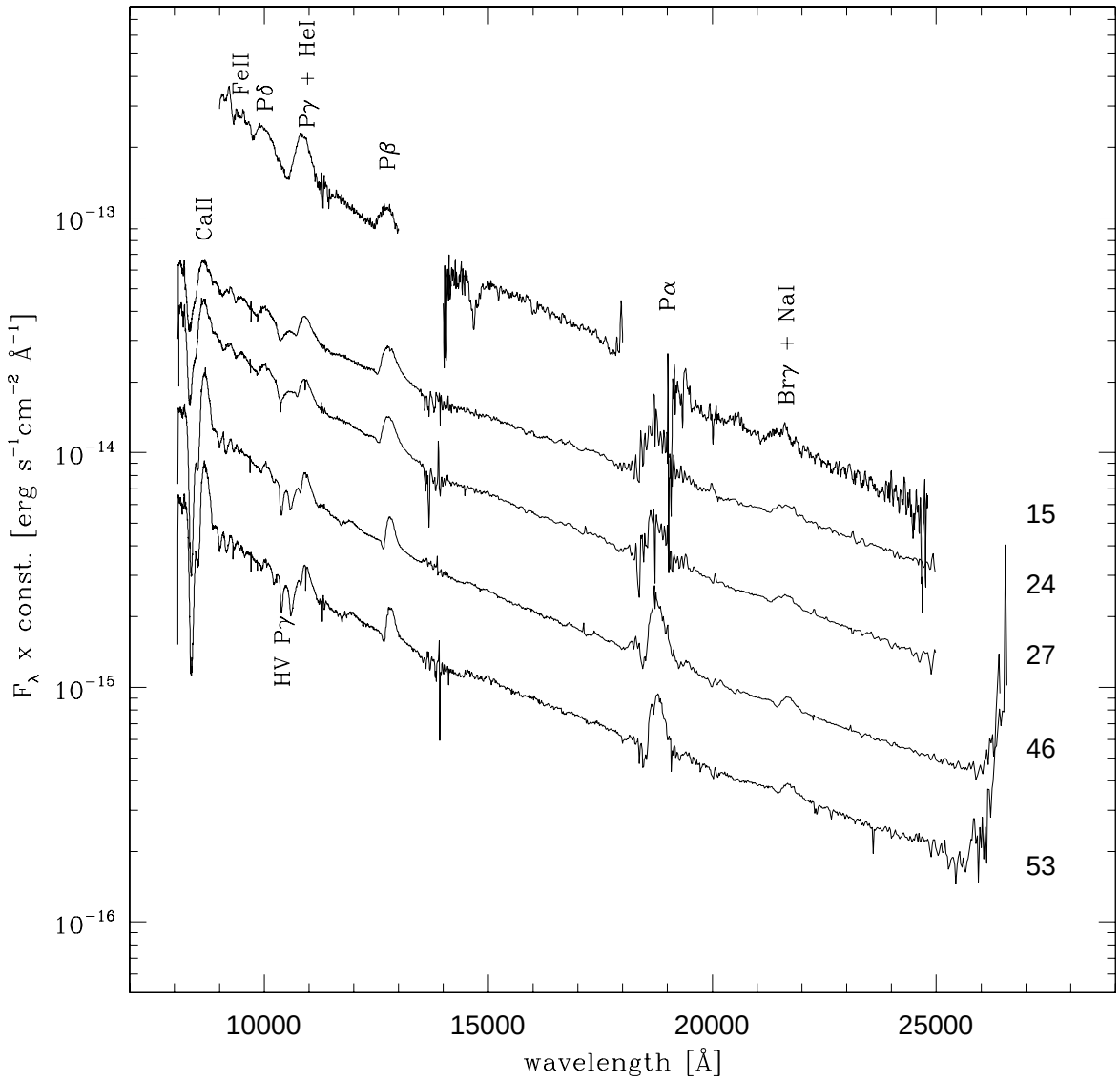
CaII
FeII
Pδ
Pγ + HeI
Pβ
Pα
Brγ + NaI
HV Pγ
15
24
27
46
53
10^{-13}
10^{-14}
10^{-15}
10^{-16}
F_λ x const. [erg $s^{-1}cm^{-2}$ $Å^{-1}$]
10000
15000
20000
25000
wavelength [Å]

Fig. 14.—

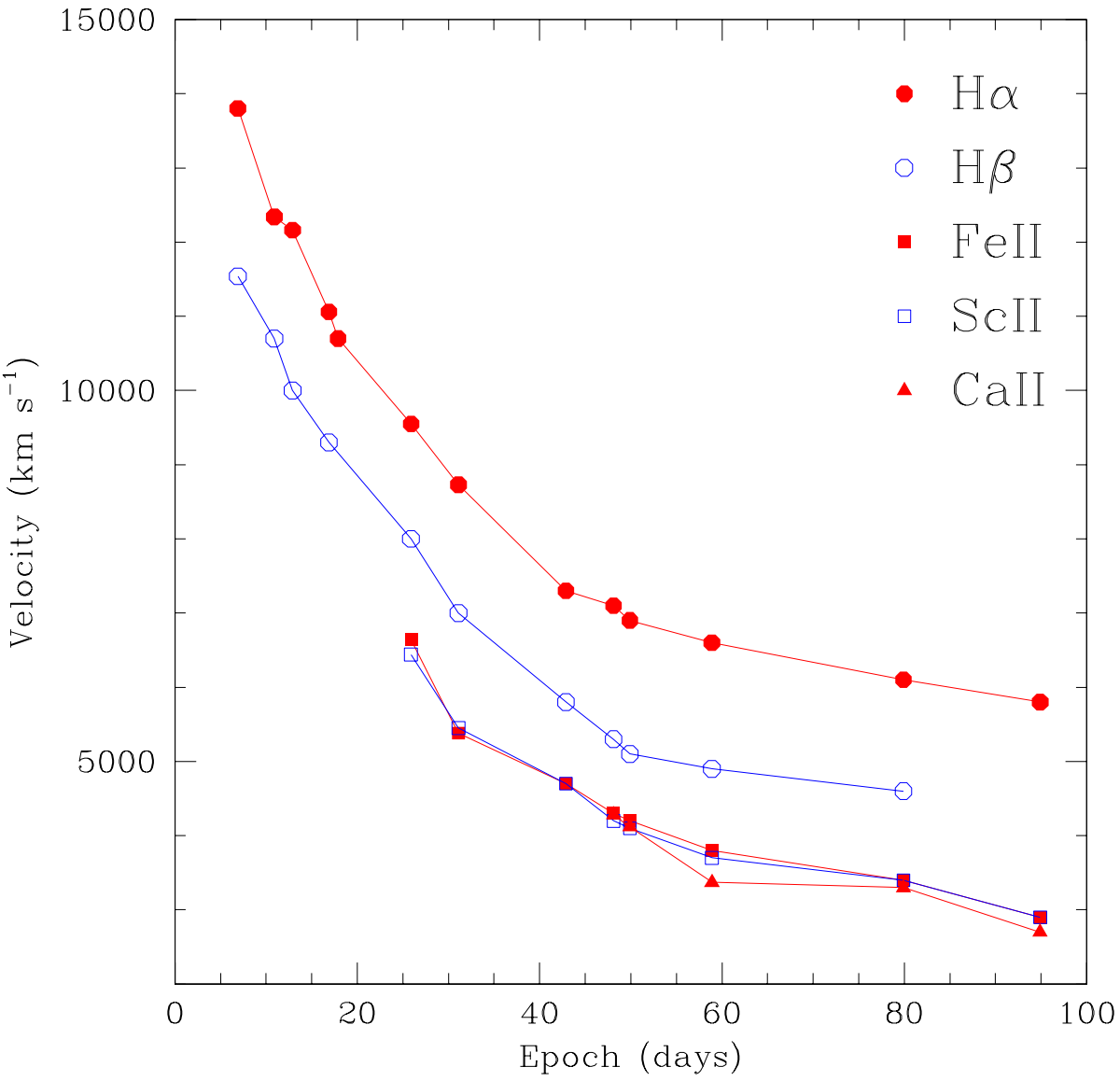

Fig. 15.— Line velocity evolution, estimated from the Doppler shift of the absorption minima, of Hα, Hβ, FeII (5169), ScII (6256), and CaII (8520).

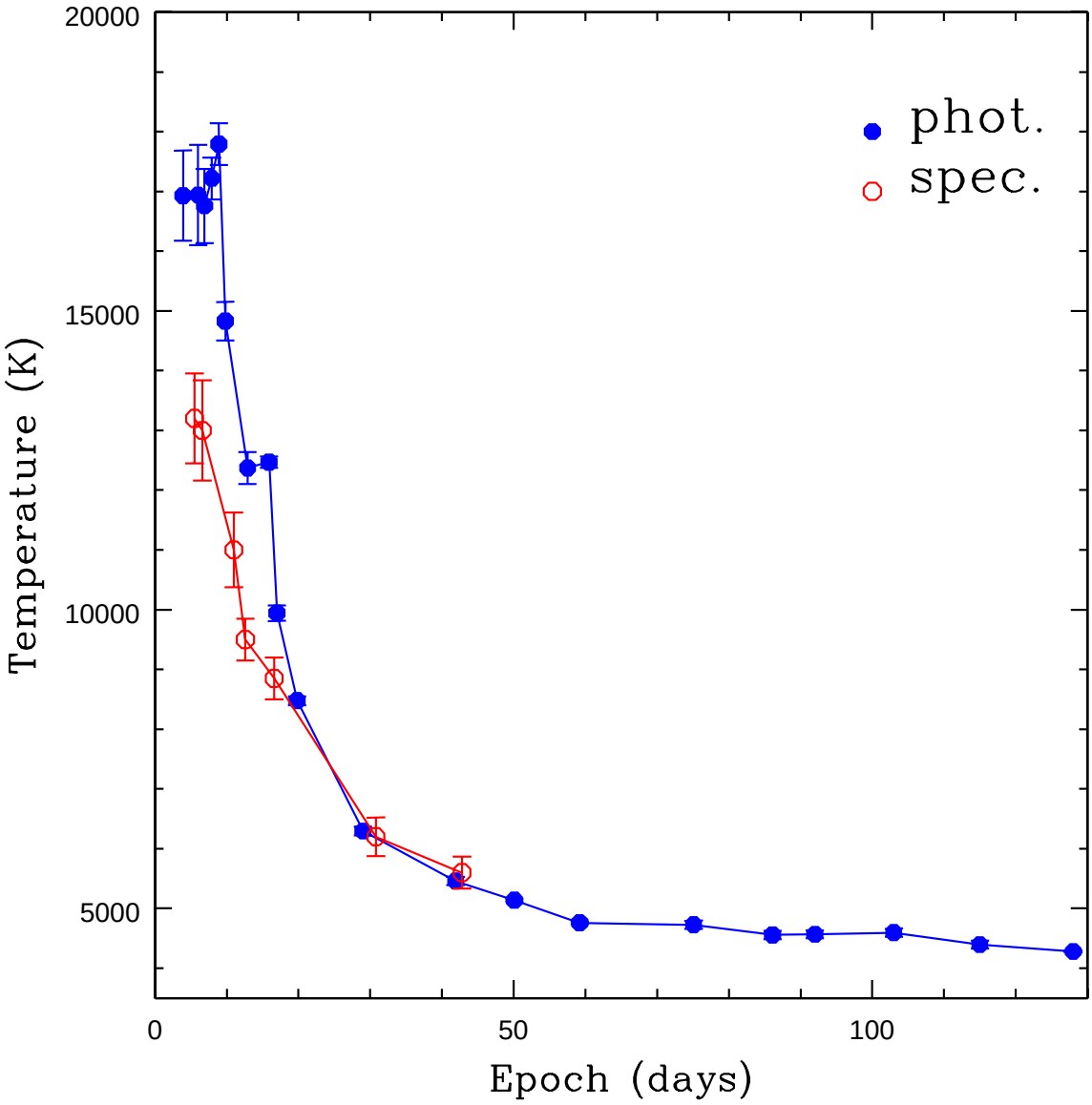

Fig. 16.— Temperature evolution of SN 2012aw, derived from blackbody fits to the observed fluxes in the range from the Swift *uvw*2- to the *K*-bands (blue filled circles) and from the continuum of selected spectra (red open circles).

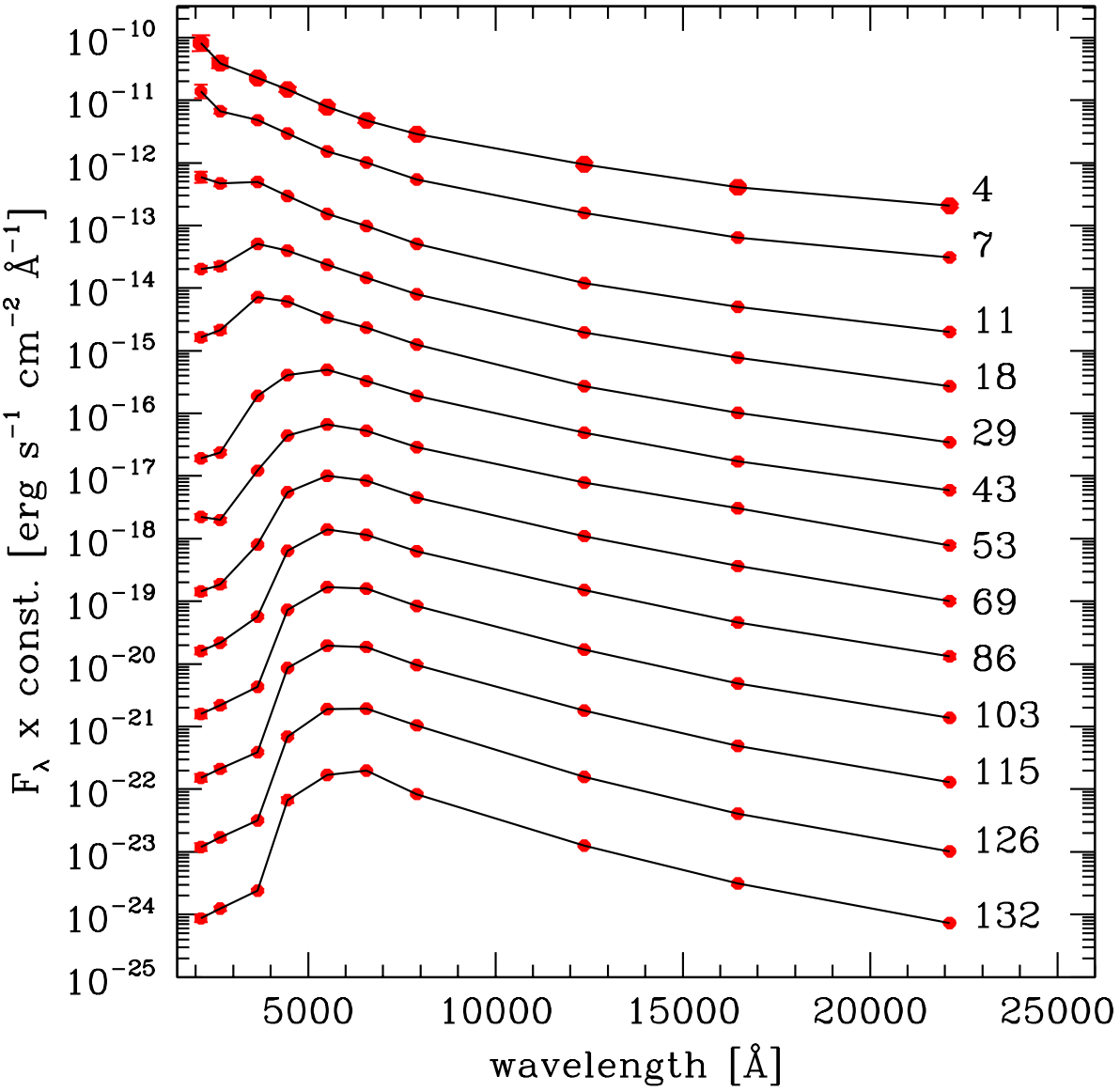

Fig. 17.— Time evolution od the spectral energy distribution of SN2012aw. Red filled circles depict the fluxes at the effective wavelengths of the photometric filters. Individual points are connected by solid black lines for clarity. Numbers mark the epochs.